Review Article

ADVANCED PHOTONICS

Generation of polarization and phase singular beams in fibers and fiber lasers

Dong Mao,[a] Yang Zheng,[a] Chao Zeng,[a] Hua Lu,[a] Cong Wang,[b] Han Zhang,[b] Wending Zhang,[a,*] Ting Mei,[a] and Jianlin Zhao[a]

[a]Northwestern Polytechnical University, School of Physical Science and Technology, MOE Key Laboratory of Material Physics and Chemistry Under Extraordinary Conditions, and Shaanxi Key Laboratory of Optical Information Technology, Xi'an, China

[b]Shenzhen University, Collaborative Innovation Centre for Optoelectronic Science and Technology, Key Laboratory of Optoelectronic Devices and Systems of Ministry of Education and Guangdong Province, Shenzhen, China

Abstract. Cylindrical vector beams and vortex beams, two types of typical singular optical beams characterized by axially symmetric polarization and helical phase front, possess the unique focusing property and the ability of carrying orbital angular momentum. We discuss the formation mechanisms of such singular beams in few-mode fibers under the vortex basis and show recent advances in generating techniques that are mainly based on long-period fiber gratings, mode-selective couplers, offset-spliced fibers, and tapered fibers. The performances of cylindrical vector beams and vortex beams generated in fibers and fiber lasers are summarized and compared to give a comprehensive understanding of singular beams and to promote their practical applications.

Keywords: cylindrical vector beam; vortex beam; orbital angular momentum; two-mode fiber; fiber laser; beam shaping.

Received Jul. 27, 2020; revised manuscript received Oct. 15, 2020; accepted for publication Nov. 17, 2020; published online Jan. 1, 2021.

[DOI: 10.1117/1.AP.3.1.014002]

1 Introduction

In the past decades, spatially modulated structured light has captured a great deal of research interest and found a variety of applications.[1–5] Spatially modulated structured light refers to light beams with special intensity, phase, or polarization distributions in the spatial domain, such as Bessel beams, Airy beams, cylindrical vector beams (CVBs), and vortex beams (VBs). Ideally, the Bessel beam represents a perfect diffraction-free optical field with a sharply defined central maximum, and thus the transverse intensity distribution is independent of the propagation distance.[6] Airy beam is another type of diffraction-free waves and displays a distinctive self-accelerating property during the propagation.[7] CVBs are generally characterized by axially symmetric polarizations and can be classified as an azimuthally polarized beam (APB), a radially polarized beam (RPB), and a hybridly polarized beam.[8,9] VBs are characterized by helical wavefronts[10–13] and are capable of carrying orbital angular momentum (OAM) because their equiphase surfaces rotate around the propagation direction, enabling the potential to develop OAM multiplexing communications.[14–16] As CVBs and VBs possess a polarization singularity and phase singularity, respectively,[9] they are also termed as singular beams and exhibit a similar doughnut-like intensity profile with a dark area at the center.[17,18]

Spatially modulated structured light was first generated in free space based on discrete bulk-state elements. Durnin et al.[19] demonstrated a zero-order Bessel beam by illuminating collimated light on a circular slit located in the focal plane of a lens. Siviloglou et al.[20] achieved an Airy beam by imposing a cubic phase to a broad Gaussian beam with a computer-controlled liquid crystal spatial light modulator. Simultaneously, various techniques and elements were developed to generate CVBs and VBs. For instance, spatial light modulators,[21,22] axial birefringent components,[23–25] specially designed laser cavities,[26–28] interferometric methods,[29–32] and nanostructured holograms[33] have been proposed to convert Gaussian beams into CVBs or to directly emit CVBs. At the same time, photopatterning of liquid crystals,[34,35] spiral phase plates,[36,37] computer generated holograms,[38] microresonators or subwavelength gratings,[39] helically twisted fibers,[40] as well as plasmonic metasurfaces[41–44] were developed to generate VBs. However, most of these beam

*Address all correspondence to Wending Zhang, zhangwd@nwpu.edu.cn

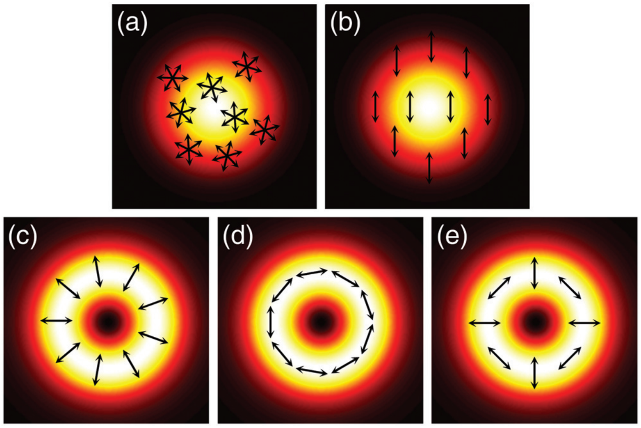

Fig. 1 Polarization distribution of (a) natural, unpolarized light, (b) linearly polarized beam, (c) RPB, (d) APB, and (e) hybridly polarized beam.

conversion or modulation systems are based on discrete components, and the complexity in optical alignment makes them difficult to use in constructing compact, low-loss, and long-haul systems.

Recently, the generation and modulation of CVBs/VBs in few-mode fibers and fiber lasers have attracting rising interests as such components or systems are compatible with optical fiber links, and this article reviews the important advances of the new emerging field. Section 2 is a brief introduction of CVBs and VBs and compares the two singular beams with several typical light beams. Following the brief introduction, Sec. 3 reviews the generation of CVBs in fibers and fiber lasers, which mainly focuses on formation principles, experimental setups, and output properties of the singular beams. In Sec. 4, we discuss corresponding contents of VBs in fibers and fiber lasers. Section 5 is a summarization of this review and discusses the perspective of CVBs and VBs in fiber-based systems.

2 Brief Introduction of CVBs and VBs

2.1 Cylindrical Vector Beams

In general, natural light has a randomly distributed polarization state as the phase and wave vector of each lightwave evolve independently in the observed spatial plane, as shown in Fig. 1(a). However, laser beams emitted from typical cavities usually exhibit identical polarization states. For example, the output beams can be linearly polarized [Fig. 1(b)], elliptically polarized, or circularly polarized, and all of them have fixed polarization orientations in the spatial plane. Different from standard laser beams or natural lights, CVBs exhibit axially symmetric polarizations in the spatial domain.[45–47] As shown in Figs. 1(c)–1(e), depending on the spatial distribution of the polarization, CVBs can be classified as RPBs, APBs, and hybridly polarized beams. As the polarization direction cannot be determined at the beam center, the CVBs show a polarization singularity and have a doughnut-like intensity profile. The focusing properties of linearly polarized Gaussian beams and RPBs are quite different when they pass through a high-numerical-aperture lens. The focused RPB has a strong longitudinal electric-field component, and the spot size reaches $0.16\lambda^2$ which is much smaller than the focused Gaussian beam $(0.26\lambda^2)$.[48] Attributing to the unique focusing property, RPBs have found numerous practical applications, such as the particle manipulation,[49] plasmonic nanofocusing,[50] high-resolution optical microscopy,[51] and high-sensitivity Z-scan techniques.[52]

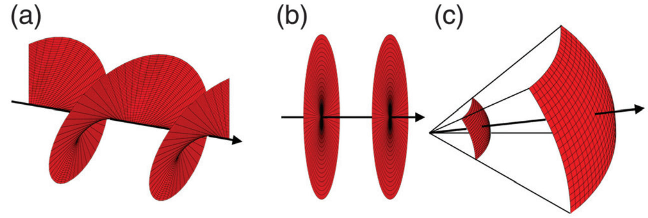

Fig. 2 Phase evolution of (a) VB, (b) plane wave, and (c) spherical wave.

2.2 Vector Beams

It is well known that plane lightwaves and spherical lightwaves exhibit plane and spherical equiphase surfaces. Unlike the plane wave or the spherical wave, VBs have a helical phase given by $\exp(il\varphi)$, where φ is the azimuthal angle, and l is the topological charge that indicates the winding number of the phase front in a single optical cycle. Figures 2(a)–2(c) show the phase evolution of VBs, plane waves, and spherical waves during propagation in an isotropic medium. The equiphase surface of a VB rotates around the propagation direction, and thus a VB carries OAM in the spatial domain.[53,54] As the phase is undetermined at the beam center, a VB shows a phase singularity and is therefore termed as a phase singular beam. Although the CVB and VB exhibit a similar doughnut-like intensity profile, they are intrinsically two different types of beams. In general, the polarization distribution of a CVB is tested by passing it through a rotating linear polarizer, while the phase property of VB is investigated by interfering it with a plane lightwave or a spherical lightwave. It should be pointed out that VBs can be linearly polarized,[55] circularly polarized,[56] and cylindrically polarized.[57] Due to the distinct phase and intensity distributions, VBs have also found widespread applications in mode division multiplexing,[58–61] optical imaging,[62] optical micromanipulation,[63–65] fabrication of magnetic three-dimensional tubular micromotors,[66] or twisted metal nanostructures,[1,67] quantum optics,[68] rotation detection,[69,70] etc. The generation methods and applications of CVBs and VBs in free space have been discussed and summarized exhaustively by several reviews and articles.[9,13,17,71–74] The following parts of this review mainly focus on the generation and application of CVBs and VBs based on few-mode fibers and fiber lasers.

3 Generation of CVBs in Fibers and Fiber Lasers

Generation of CVBs in fibers and fiber lasers is mainly based on the exciting and extracting of desired eigenmodes in few-mode fibers such as two-mode fiber (TMF) and four-mode fiber. The spatial properties of TMF lasers are completely different from fiber lasers based on a single-mode fiber (SMF).[75–79] As shown in Fig. 3, taking TMF as an example, it can guide the LP_{01} mode and LP_{11} mode in the scalar approximation. When accounting for the polarization distribution, the LP_{01} mode includes two degenerate fundamental modes (HE_{11}^x and HE_{11}^y) that have the same effective refractive index but orthogonal polarization

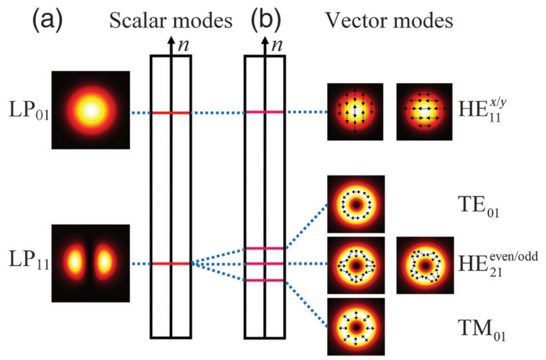

Fig. 3 Mode distributions of TMF under (a) scalar approximation and (b) corresponding groups of the vector modes. Adapted with permission from Ref. 80 © OSA Publishing.

states. The LP_{11} mode includes four vector modes,[81] i.e., TE_{01}, TM_{01}, and $HE_{21}^{even/odd}$. Among them, HE_{21}^{even} and HE_{21}^{odd} are strictly degenerated modes with the same effective refractive index while orthogonal polarization states, and TM_{01} and TE_{01} modes are separated by HE_{21} modes and have slightly different effective refractive indices.

To investigate the coupling characteristic between fundamental modes ($HE_{11}^{x/y}$) and the first group high-order modes ($HE_{21}^{even/odd}$, TM_{01}, and TE_{01}), it is more convenient to introduce the so-called vortex basis sets:[82]

$$\begin{aligned}
V_{11}^{+}(r,\theta)&=(HE_{11}^{x}+iHE_{11}^{y})/\sqrt{2}=(\hat{x}+i\hat{y})F_{01}/\sqrt{2},\\
V_{11}^{-}(r,\theta)&=(HE_{11}^{x}-iHE_{11}^{y})/\sqrt{2}=(\hat{x}-i\hat{y})F_{01}/\sqrt{2},\\
V_{21}^{+}(r,\theta)&=(HE_{21}^{even}+iHE_{21}^{odd})/\sqrt{2}=e^{i\theta}(\hat{x}+i\hat{y})F_{11}/\sqrt{2},\\
V_{21}^{-}(r,\theta)&=(HE_{21}^{even}-iHE_{21}^{odd})/\sqrt{2}=e^{-i\theta}(\hat{x}-i\hat{y})F_{11}/\sqrt{2},\\
V_{T}^{+}(r,\theta)&=(TM_{01}-iTE_{01})/\sqrt{2}=e^{-i\theta}(\hat{x}+i\hat{y})F_{11}/\sqrt{2},\\
V_{T}^{-}(r,\theta)&=(TM_{01}+iTE_{01})/\sqrt{2}=e^{i\theta}(\hat{x}-i\hat{y})F_{11}/\sqrt{2}.
\end{aligned}\tag{1}$$

Here, $\hat{x}$ and $\hat{y}$ represent linear polarizations along the x axis and y axis of the TMF, F_{01} and F_{11} are radial wave functions of the LP_{01} and LP_{11} modes, and θ is the azimuthal coordinate, respectively. Thus, in vortex basis sets, the six vector modes can be rewritten as

$$\begin{aligned}
HE_{11}^{x}&=\hat{x}F_{01},\\
HE_{11}^{y}&=\hat{y}F_{01},\\
HE_{21}^{even}&=(\hat{x}\cos\theta-\hat{y}\sin\theta)F_{11},\\
HE_{21}^{odd}&=(\hat{x}\sin\theta+\hat{y}\cos\theta)F_{11},\\
TM_{01}&=(\hat{x}\cos\theta+\hat{y}\sin\theta)F_{11},\\
TE_{01}&=(\hat{x}\sin\theta-\hat{y}\cos\theta)F_{11}.
\end{aligned}\tag{2}$$

Because TM_{01} and TE_{01} modes are exactly RPB and APB, respectively, the generation of CVBs in fibers and fiber lasers comes down to the excitation and extraction of the TM_{01} or TE_{01} mode. The mode couplers are key elements to generate CVB and VB, and the fiber-based mode couplers mainly include long period fiber gratings (LPFGs), fiber-fused mode-selective couplers, offset-spliced fibers, and tapered fibers. The properties of these mode couplers and performances of CVBs are discussed in the following parts.

3.1 Long Period Fiber Grating for Generating CVBs

When the refractive index of the fiber is periodically modulated along the propagation direction of light, the fundamental mode can be coupled into the copropagating high-order modes based on the following coupling equations:[83,84]

$$\begin{aligned}
\frac{dA_1(z)}{dz}&=i\delta A_1(z)+i\kappa A_2(z),\\
\frac{dA_2(z)}{dz}&=i\delta A_2(z)+i\kappa A_1(z),
\end{aligned}\tag{3}$$

where $A_1(z)$ and $A_2(z)$ represent complex amplitudes of the fundamental mode and the desired high-order mode, and κ is the coupling coefficient between two modes. δ is the mismatch of two wave vectors and can be expressed as $\delta=\beta_1-\beta_2-K$, in which $\beta_1=2\pi n_{eff1}/\lambda$ and $\beta_2=2\pi n_{eff2}/\lambda$ are propagation constants while n_{eff1} and n_{eff2} are effective refractive indices of the fundamental mode and high-order mode. λ is the wavelength, and $K=2\pi/\Lambda$ is the wave vector of the fiber grating with a period of Λ.

To realize effective coupling of the fundamental mode and the desired high-order mode, the phase match condition must be satisfied so that the coupling coefficient reaches critical coupling state. Thus, the mismatch δ should be zero, and the period of fiber grating is $\Lambda=\lambda/(n_{eff1}-n_{eff2})$. As the difference $(n_{eff1}-n_{eff2})$ of effective refractive indices between two modes is relatively small ($\sim 10^{-2}$ to 10^{-3}), the period of the fiber grating for mode conversion is hundreds of micrometers at the wavelength of 1.55 μm.

The coupling coefficient κ between $HE_{11}^{x/y}$ and the first group high-order vector modes (TE_{01}, $HE_{21}^{even/odd}$, and TM_{01}) can be expressed as[80,84]

$$\kappa=\frac{\pi}{\lambda}\sqrt{\frac{\varepsilon_0}{\mu_0}}n_0\iint \mathbf{E}_i(x,y)\cdot\Delta n(x,y)\mathbf{E}_j(x,y)\,dx\,dy,\tag{4}$$

where $\mathbf{E}_i(x,y)$ and $\mathbf{E}_j(x,y)$ are the transverse electric fields of the fundamental mode and the desired high-order mode, respectively, n_0 is the refractive index of fiber core, and ε_0 and μ_0 are the permittivity and permeability of vacuum, respectively. By substituting Eq. (2) into Eq. (4), the coupling coefficient between $HE_{11}^{x/y}$ and $HE_{21}^{even/odd}$ ($HE_{11}^{x}\leftrightarrow HE_{21}^{even}$) is obtained as

$$\begin{aligned}
\kappa_1=\frac{\pi}{\lambda}\sqrt{\frac{\varepsilon_0}{\mu_0}}n_0\iint &\hat{x}F_{01}(r)\Delta n(r,\theta)(\hat{x}\cos\theta\\
&-\hat{y}\sin\theta)F_{11}(r)r\,dr\,d\theta.
\end{aligned}\tag{5}$$

If the modulation of the refractive index evolves independently with the azimuthal angle θ and radius r such that $\Delta n(r,\theta)=\Delta n(r)\Delta n(\theta)$, the coupling coefficient takes the form:[80]

$$\kappa_1=\frac{\pi}{\lambda}\sqrt{\frac{\varepsilon_0}{\mu_0}}n_0\int F_{01}(r)\Delta n(r)F_{11}(r)r\,dr\int\Delta n(\theta)\cos\theta\,d\theta.\tag{6}$$

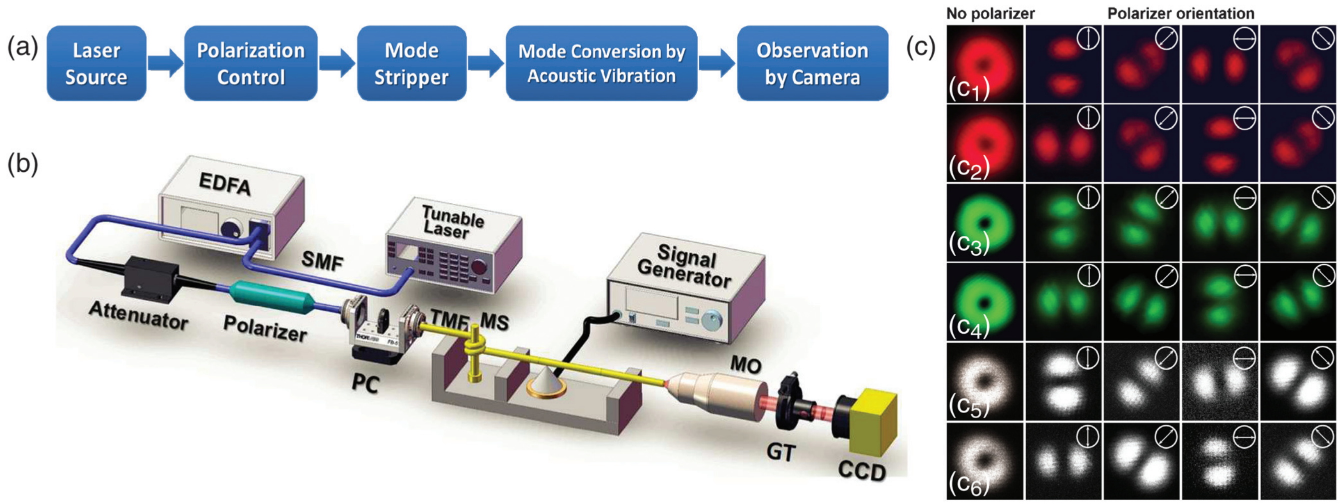

Fig. 4 (a) Flow diagram and (b) experimental setup for generating CVBs based on an acoustically induced LPFG. SMF, single-mode fiber; EDFA, erbium-doped fiber amplifier; PC, polarization controller; TMF, two-mode fiber; MS, mode stripper; MO, micro-objective; GT, Glan–Taylor prism polarizer; CCD, charge coupled device. (c) Intensity patterns of (c_1), (c_3), (c_5) RPB and (c_2), (c_4), (c_6) APB at (c_1), (c_2) 633 nm, (c_3), (c_4) 532 nm, and (c_5), (c_6) 1550 nm before and after passing a polarizer. Adapted with permission from Ref. 80 © OSA Publishing.

Similarly, the coupling coefficient κ_2 ($\mathrm{HE}_{11}^{x}\leftrightarrow\mathrm{HE}_{21}^{\mathrm{odd}}$), κ_3 ($\mathrm{HE}_{11}^{x}\leftrightarrow\mathrm{TE}_{01}$), κ_4 ($\mathrm{HE}_{11}^{x}\leftrightarrow\mathrm{TM}_{01}$), κ_5 ($\mathrm{HE}_{11}^{y}\leftrightarrow\mathrm{HE}_{21}^{\mathrm{even}}$), κ_6 ($\mathrm{HE}_{11}^{y}\leftrightarrow\mathrm{HE}_{21}^{\mathrm{odd}}$), κ_7 ($\mathrm{HE}_{11}^{y}\leftrightarrow\mathrm{TE}_{01}$), κ_8 ($\mathrm{HE}_{11}^{y}\leftrightarrow\mathrm{TE}_{01}$) are

$$\begin{aligned}
\kappa_2 &= \frac{\pi}{\lambda}\sqrt{\frac{\varepsilon_0}{\mu_0}}n_0\int F_{01}(r)\Delta n(r)F_{11}(r)r\mathrm{d}r\int \Delta n(\theta)\sin\theta\mathrm{d}\theta,\\
\kappa_3 &= \frac{\pi}{\lambda}\sqrt{\frac{\varepsilon_0}{\mu_0}}n_0\int F_{01}(r)\Delta n(r)F_{11}(r)r\mathrm{d}r\int \Delta n(\theta)\sin\theta\mathrm{d}\theta,\\
\kappa_4 &= \frac{\pi}{\lambda}\sqrt{\frac{\varepsilon_0}{\mu_0}}n_0\int F_{01}(r)\Delta n(r)F_{11}(r)r\mathrm{d}r\int \Delta n(\theta)\cos\theta\mathrm{d}\theta,\\
\kappa_5 &= -\frac{\pi}{\lambda}\sqrt{\frac{\varepsilon_0}{\mu_0}}n_0\int F_{01}(r)\Delta n(r)F_{11}(r)r\mathrm{d}r\int \Delta n(\theta)\sin\theta\mathrm{d}\theta,\\
\kappa_6 &= \frac{\pi}{\lambda}\sqrt{\frac{\varepsilon_0}{\mu_0}}n_0\int F_{01}(r)\Delta n(r)F_{11}(r)r\mathrm{d}r\int \Delta n(\theta)\cos\theta\mathrm{d}\theta,\\
\kappa_7 &= -\frac{\pi}{\lambda}\sqrt{\frac{\varepsilon_0}{\mu_0}}n_0\int F_{01}(r)\Delta n(r)F_{11}(r)r\mathrm{d}r\int \Delta n(\theta)\cos\theta\mathrm{d}\theta,\\
\kappa_8 &= \frac{\pi}{\lambda}\sqrt{\frac{\varepsilon_0}{\mu_0}}n_0\int F_{01}(r)\Delta n(r)F_{11}(r)r\mathrm{d}r\int \Delta n(\theta)\sin\theta\mathrm{d}\theta. \qquad (7)
\end{aligned}$$

From Eqs. (6) and (7), one can find that two integrals affect the coupling coefficient and should be non-zero simultaneously. Actually, an acoustic flexural wave propagating in the z direction with vibration along the x axis can introduce an asymmetric refractive index modulation with respect to the vibration direction in an unjacketed fiber.[80] The asymmetric refractive index distribution at the cross section of such acoustically induced LPFG is

$$\Delta n(r,\theta) = n_0 r\cos\theta. \qquad (8)$$

Therefore, the coupling coefficients between the fundamental mode and the high-order mode in the acoustically induced LPFG can be further expressed as

$$\begin{aligned}
\kappa_1 &= C\kappa_r\int_0^{2\pi}\cos^2\theta\mathrm{d}\theta = C\kappa_r\pi,\\
\kappa_2 &= C\kappa_r\int_0^{2\pi}\cos\theta\sin\theta\mathrm{d}\theta = 0,\\
\kappa_3 &= C\kappa_r\int_0^{2\pi}\cos\theta\sin\theta\mathrm{d}\theta = 0,\\
\kappa_4 &= C\kappa_r\int_0^{2\pi}\cos^2\theta\mathrm{d}\theta = C\kappa_r\pi,\\
\kappa_5 &= -C\kappa_r\int_0^{2\pi}\cos\theta\sin\theta\mathrm{d}\theta = 0,\\
\kappa_6 &= C\kappa_r\int_0^{2\pi}\cos^2\theta\mathrm{d}\theta = -C\kappa_r\pi,\\
\kappa_7 &= -C\kappa_r\int_0^{2\pi}\cos^2\theta\mathrm{d}\theta = -C\kappa_r\pi,\\
\kappa_8 &= C\kappa_r\int_0^{2\pi}\cos\theta\sin\theta\mathrm{d}\theta = 0, \qquad (9)
\end{aligned}$$

where $C = \frac{\pi}{\lambda}\sqrt{\frac{\varepsilon_0}{\mu_0}}n_0$, $\kappa_r = \int_0^r F_{01}(r)F_{11}(r)r^2\mathrm{d}r$, and both of them are constants for a certain acoustically induced LPFG. Thus, RPB and APB can be obtained by coupling the HE_{11}^{x} to TM_{01} and HE_{11}^{y} to TE_{01}, respectively.

Figures 4(a) and 4(b) show the experimental setup for generating a CVB at the wavelength of 1550 nm using the acoustically induced LPFG.[80] First, the laser was amplified by an erbium-doped fiber amplifier (EDFA), and the output beam was linearly polarized HE_{11}^{x} or HE_{11}^{y} mode after passing through a polarizer and polarization controller (PC). Then, the laser entered the TMF and was further purified as the HE_{11} mode by a mode stripper. After that, the mode conversion was implemented with an acoustically induced LPFG of which one end was glued to the tip of an acoustic transducer and the other end was fixed on a fiber clamp. The acoustic wave was imposed on the TMF with an acoustic transducer. The operation was switchable between RPB and APB via adjusting the PC, and the phase matching condition was satisfied via tuning the frequency of the acoustic wave. Figure 4(c) shows the intensity patterns of RPB and APB at the wavelength of 532, 633, and 1550 nm before and after passing a linear polarizer. The SMF-28 fiber was used as a TMF to generate CVBs at 532 and 633 nm, while the TMF (OFS: two mode step-index fiber) was used to generate CVBs at 1550 nm. This type of mode converter is capable of delivering high-purity CVBs with broadband wavelength tunability, while the entire system is quite complicated and costly for practical applications.

Based on the similar mode coupling principle, Dong and Chiang[85] fabricated a mode converter by directly writing the LPFG on TMF with a CO_2 laser. The asymmetrical index distribution in the fiber core induced by the laser enabled the coupling of the fundamental mode to the high-order cylindrical vector mode. The LPFG with 15 grating periods exhibited a conversion efficiency higher than 99% from 1529.1 to 1563.1 nm. The broad conversion bandwidth was induced by the slight variation of the grating period during the fabrication. By adjusting the polarization state of the input HE_{11} mode, four cylindrical vector modes (TE_{01}, HE_{21}^{even}, HE_{21}^{odd}, TM_{01}) can be obtained from the LPFG. Furthermore, the cascading chirped LPFGs and dual-resonance LPFG were proposed to enlarge the bandwidth of the mode converter, enabling the capability of wavelength-tunable CVB generation in fibers or fiber lasers.[86–88] Such LPFG-based mode converters possess obvious advantages of low loss, small reflection, and high fabrication flexibility.

In the aforementioned works, the CVBs were formed external to the laser cavity by modulating the transverse modes in TMFs. By incorporating the LPFG into a fiber resonator, CVBs can also be directly generated from fiber lasers. Chen et al[89] demonstrated an all-fiber laser delivering CVBs based on the combination of an LPFG and a two-mode fiber Bragg grating (TMFBG). The mode conversion was realized by the LPFG, and the mode purity of CVBs was higher than 98%. In their scheme, the TMFBG played double roles of a mode selector to extract the CVBs from hybrid modes and a spectral filter to fix the laser wavelength. The lasing threshold and slope efficiency of the laser were 24.5 mW and 35.41%, respectively. The authors have also demonstrated that the resonance efficiency of the cylindrical vector laser experienced a sudden increase from 13.26% to 32.48% when the pump reached a threshold power, and this phenomenon was attributed to the transversal hole burning effect in the double-clad Yb-doped fiber.[90]

3.2 Mode-Selective Coupler for Generating CVBs

Micronano fiber is an important element for ultrafast fiber lasers and micronano optics,[91–93] and it can also be used to actualize mode-selective couplers based on the coupling of evanescent field. The typical mode-selective couplers include fiber-polished couplers and fiber-fused couplers, and both of them are based on the mode coupling of closely spaced fibers.[94–96] For fiber-fused couplers, as shown in Fig. 5, the coupling equation is presented as Eq. (10), which is similar to Eq. (3) but has different mismatch parameters.[97] It should be noted that Eq. (10) is only suitable for weakly fused fibers. In this case, $\delta_1 = \beta_1 + C_{11}$ and $\delta_2 = \beta_2 + C_{22}$, where β_1 and β_2 are previously defined propagation constants of the fundamental mode and the high-order mode, respectively, C_{11} and C_{22} are self-coupling coefficients, and κ is the mutual-coupling coefficient. The self-coupling

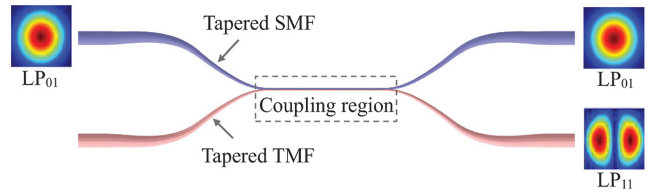

Fig. 5 Mode-selective coupler based on tapered SMF and TMF.

coefficient only results in the change of the effective index and thus the phase matching condition, while it has no impact on the coupled power between modes. To realize effective mode coupling, the phase matching condition should also be satisfied ($\Delta\delta = \delta_1 - \delta_2 = 0$),[97] indicating that β_1 should be equal to β_2. However, SMF and TMF have different parameters, and generally, the two propagation constants β_1 and β_2 have different values.

$$\frac{\mathrm{d}A_1(z)}{\mathrm{d}z} = i\delta_1 A_1(z) + i\kappa A_2(z),$$
$$\frac{\mathrm{d}A_2(z)}{\mathrm{d}z} = i\delta_2 A_2(z) + i\kappa A_1(z). \tag{10}$$

Based on the finite element simulation, Wan et al.[97] demonstrated that the best diameter ratio between the SMF and TMF should be 0.63 to satisfy the phase-matching condition. To simplify the calculation, they assumed that four high-order vector modes had the same propagation constant and coupling efficiency. In their experiment, the diameter of the SMF was pretapered to 79 μm, and the mode-selective coupler was fabricated by a weak fusion technique. At the wavelength of 1550 nm, the purity of the vector mode was measured to be about 97% by the tight bend approach. When incorporating the mode-selective coupler into a figure-8 fiber laser, both RPB and APB have been obtained from the TMF terminal of the mode-selective coupler through adjusting the polarization state. The central wavelength, spectral bandwidth, pulse duration, and repetition rate were 1556.3 nm, 3.2 nm, 17 ns, and 0.66 MHz, respectively. With the assistance of a carbon nanotube saturable absorber, they have achieved femtosecond dual-wavelength soliton mode locking in a ring fiber laser, further confirming the broadband operating characteristics of the mode-selective coupler.[98] After that, they demonstrated an all-fiber CVB laser based on a symmetric TMF coupler for both high-order mode excitation and splitting.[99]

In the aforementioned CVB fiber lasers,[97,98,100] the fiber resonators were composed of SMF components, and the fundamental mode was converted into the high-order mode by the mode-selective coupler. Wang et al.[101] proposed a wavelength division-multiplexing mode-selective coupler that converted the LP_{01} mode in the SMF to the LP_{11} mode in the TMF and combined the LP_{11} modes in the TMF at wavelengths of 980 and 1550 nm. In the fabrication process, the diameter of the SMF was pretapered to 77.5 μm, carefully aligned with the TMF, and then fused together with the flame brushing technique. As shown in Fig. 6, based on the TMF components of the EDF, coupler, and WDM, they constructed an all-fiber laser and observed the LP_{11} mode and CVBs with a modal purity higher than 95%. By injecting a picosecond laser pulse into the cavity with a mode-selective coupler, they observed a direct oscillation of the LP_{11} mode with an output power of 4 mW in

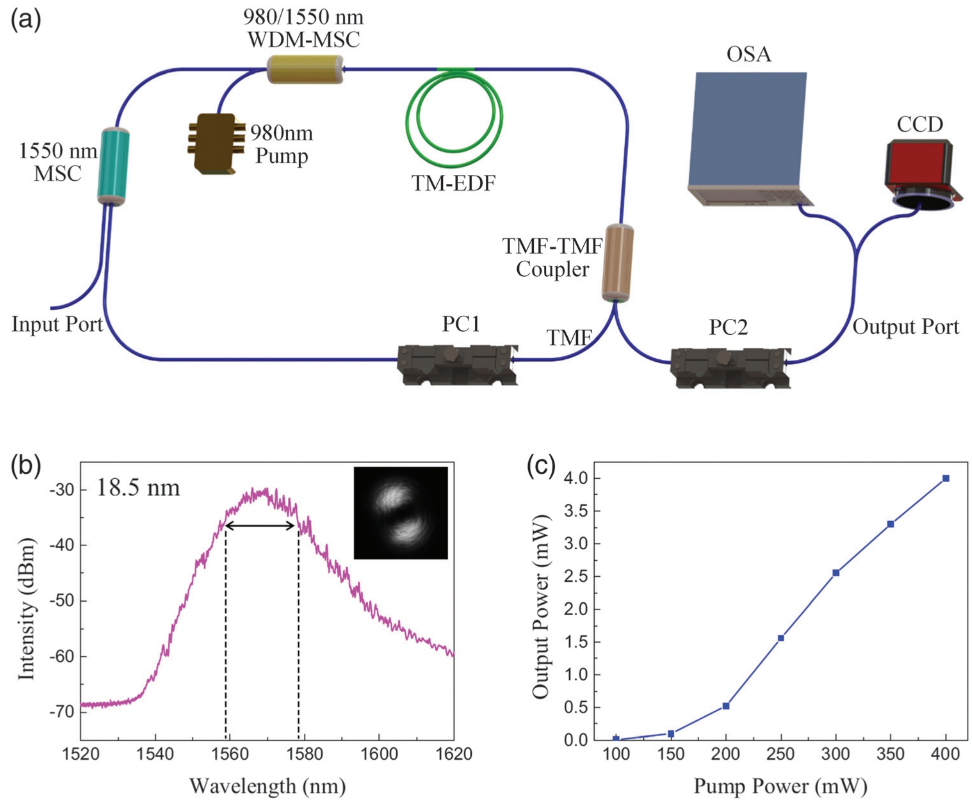

Fig. 6 (a) Configuration of the all-TMF laser for LP_{11} mode oscillation. TM-EDF, two-mode erbium-doped fiber; PC, polarization controller; OSA, optical spectrum analyzer; CCD, charge coupled device; MSC, mode-selective coupler; WDM, wavelength division multiplexer. (b) Spectrum of the TMF laser; the inset shows the near-field pattern of the generated LP_{11} mode. (c) The relationship between the pump and output powers. Adapted with permission from Ref. 101 © OSA Publishing.

the all TMF laser. Based on the similar mode-selective couplers, several high-order modes including CVBs and VBs have been achieved at the wavelength of 1.0 μm in all-fiber Yb-doped lasers.[102]

3.3 Offset-Spliced Fiber and Tapered Fiber for Generating CVBs

For mode-selective couplers and LPFGs, the parameters such as the fiber diameter and grating period should be precisely controlled to generate the desired CVBs. According to the mode matching theory, when the input mode in the SMF deviates from the axial symmetry with respect to the TMF, a part of the fundamental mode will couple into high-order modes. The coupling efficiency is obtained via calculating the overlap between the modes in the SMF and TMF.[103] Thus, offset splicing the SMF and TMF can work as a simple and effective mode-coupling element. By offset aligning the SMF and TMF, Grosjean et al.[104] excited the RPB while still observing the residual fundamental mode. The fundamental mode can be greatly reduced to heighten the purity of the RPB with the enhancement of the mismatch between two fibers. However, the loss also enlarged exponentially with the increase of the mismatch, which limited the conversion efficiency of the device.

We investigated the coupling behavior of the offset-spliced SMF and TMF based on the finite element analysis method.[105] Figure 7(a) shows the sketch map of the offset-spliced fiber, in which the light is injected from the SMF terminal and output from the TMF terminal. Figures 7(b) and 7(c) show that the coupling efficiency from the fundamental mode to the TM_{01} or TE_{01} modes dramatically increased with the enlargement of the mismatch distance when $\Delta R < 5.2$ μm. Taking TM_{01} mode as an example, when ΔR approached 5.2 μm, the electric field of the TM_{01} mode strongly overlapped with that of HE^{y}_{11} and there existed a maximal coupling efficiency of 20.7%. When the mismatch distance increased further, the coupling efficiency decreased gradually due to the subsiding overlap of the two electric fields.

After the offset-spliced fiber, the fundamental mode and high-order modes coexisted in the TMFs. The mode purity can be improved by reflecting back the fundamental mode while transmitting high-order modes with a TMFBG.[106–110] The blue curve in Fig. 8(a) shows a typical reflection spectrum of the TMFBG, which had three reflection peaks at 1056.0, 1054.5, and 1053.0 nm, respectively.[108] For FBGs, the reflection wavelength $\lambda_B = 2n_{\mathrm{eff}}\Lambda$, where n_{eff} and Λ were the effective refractive index of each mode and the grating period, respectively. As the effective refractive index was different for the LP_{01} and LP_{11} modes, the TMFBG displayed three reflection peaks. Peak 1 related to the coupling of LP_{01} to LP_{01} mode, peak 2 represented that of LP_{01} to LP_{11} mode, and peak 3 denoted that of LP_{11} to LP_{11} mode, respectively. When the laser spectrum

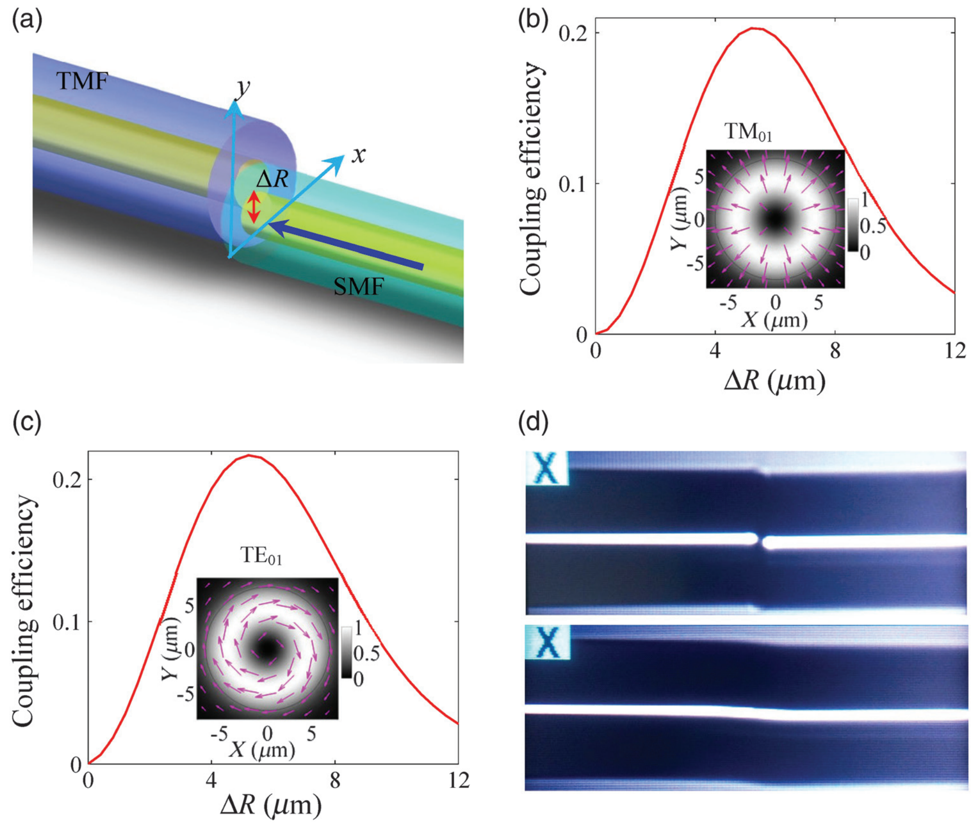

Fig. 7 (a) Diagram of the offset-spliced SMF and TMF. Calculated coupling efficiency of the fundamental mode to (b) TM_{01} mode and (c) TE_{01} mode versus mismatch distances ΔR. The polarization of the fundamental mode is (b) parallel and (c) perpendicular to the mismatch direction y, respectively. The insets show the calculated normalized intensities and polarization distributions of the TM_{01} and TE_{01} modes, respectively. (d) Measured images of the SMF and TMF before and after splicing. Adapted with permission from Ref. 105 © AIP Publishing.

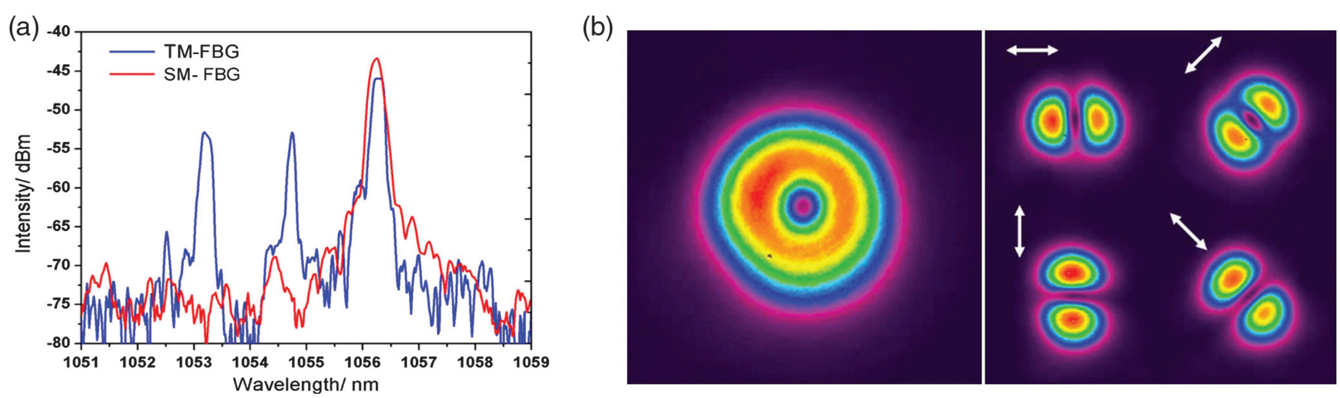

Fig. 8 (a) Reflection spectrum of TMFBG and SMFBG. (b) Intensity distribution of radially polarized laser beam before and after passing through a linear polarizer with the transmission axis orientation denoted by arrows. Adapted with permission from Ref. 108 © OSA Publishing.

was fixed by a single-mode fiber Bragg grating (SMFBG) [red curve in Fig. 8(a)] at peak 1, the fundamental mode was reflected back and the desired high-order mode was exported from the TMFBG.[111] Based on the offset-spliced fiber and TMFBG, Sun et al. constructed the figure-8 fiber laser,[108] linear-cavity fiber laser,[106,112,113] and ring fiber laser[109,114] to directly generate RPB and APB. In the temporal domain, these cylindrical vector fiber lasers were capable of delivering continuous waves, microsecond pulses, nanosecond pulses, and picosecond pulses.

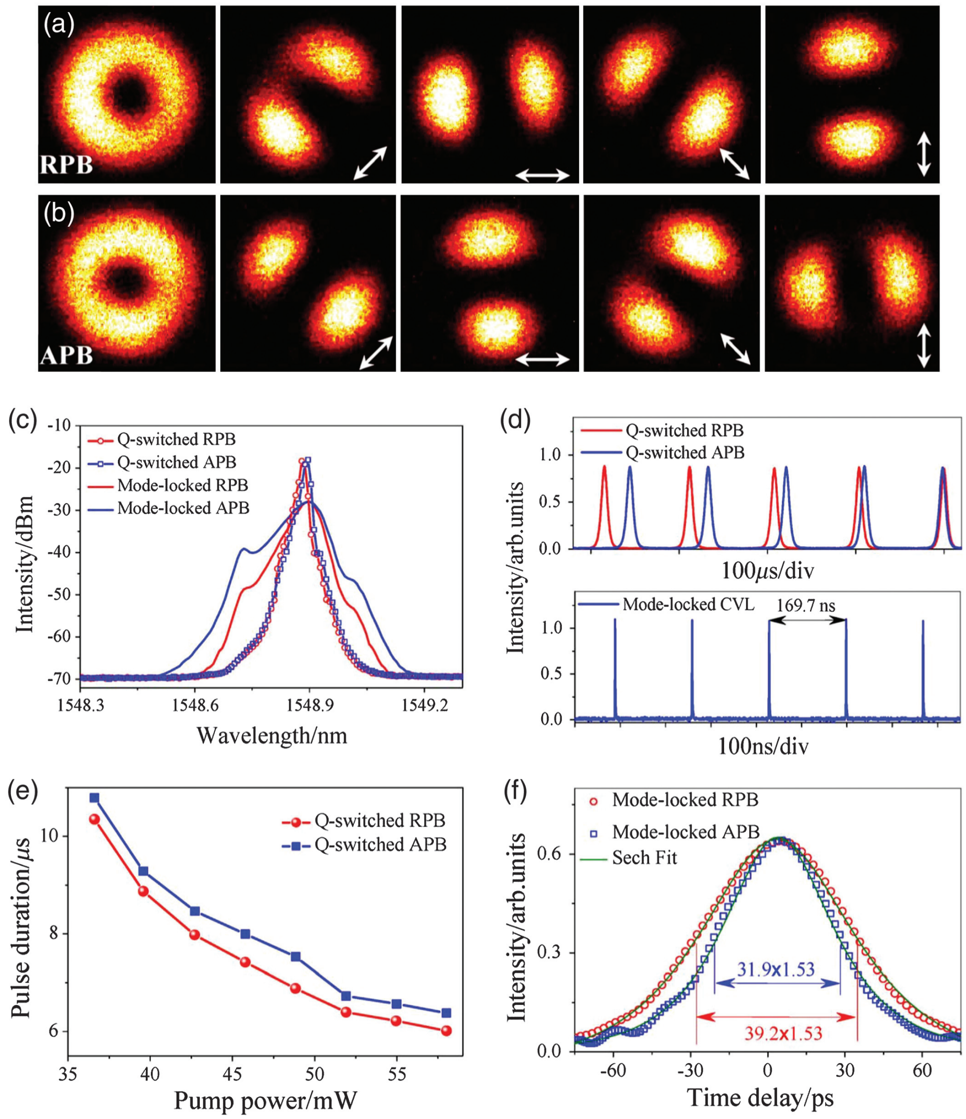

Fig. 9 *Q*-switched and mode-locked cylindrical vector beam lasers. Mode-locked (a) RPB and (b) APB before and after passing through a polarizer. (c) Optical spectra and (d) pulse trains of *Q*-switched and mode-locked cylindrical vector beam lasers. (e) Evolution of *Q*-switched cylindrical vector beam lasers. (f) Autocorrelation traces of mode-locked cylindrical vector beam lasers. Adapted with permission from Ref. 105 © AIP Publishing.

With a carbon nanotube saturable absorber, we have constructed an ultrafast all-fiber CVB laser at 1.55 μm based on an offset-spliced fiber and TMFBG.[105] The ultrafast CVB can be switched between radially and azimuthally polarized states and the pulse duration reached 6.87 ps. For the optimized lateral displacement of 4.5 μm, the coupling efficiency of the fundamental mode to TM_{01} or TE_{01} was about 20% while the insertion loss was higher than 3 dB, which limited the emission efficiency and output power of the laser. Based on the mode coupling of the tapered SMF and TMF, we proposed a new mode converter with an insertion loss of 0.36 dB to replace the offset-spliced fibers.[115] For tapered fibers, the coupling efficiency of the fundamental mode to TM_{01}/TE_{01} was 14.0%/20.6%, which was comparable with that of offset-spliced fibers. The insertion loss of the SMF-TMF taper is much lower than that of the offset-spliced fibers. The output power of the CVB laser based on tapered fibers reached ~20 mW, which was almost 1.5 to 2 times higher than that based on offset-spliced fibers. Similar to that of offset-spliced fibers, the laser was switchable between the radially and azimuthally polarized states by adjusting the input polarization in SMF, as shown in Figs. 9(a) and 9(b). In the temporal domain, the operation was tunable among continuous-wave, *Q*-switched, and mode-locked states by changing the pump strength and saturable absorber. Figures 9(c)–9(f) show the optical spectra, pulse trains, evolution of *Q*-switched lasers, and autocorrelation traces of the mode-locked pulses. The duration of *Q*-switched RPB/APB spanned from 10.4/10.8 to 6/6.4 μs by tuning the pump power, while that of the mode-locked pulse varied from 39.2/31.9 to 5.6/5.2 ps by controlling the laser bandwidth with an SMFBG.

Table 1 Generation systems and performances of CVBs using different schemes.

Coupling device	Output device	Wavelength (nm)	Mode purity	Output power (mW)	Pulse duration	Generation system	Supplementary information	Ref.
LPFG	TMF	1450/1620	99.8%	/	/	Ring-shaped fiber	Microbend grating, period: 800 μm; insertion loss: 0.05%	117
LPFG	TMF	1550/633/532	99.9%	2.4	/	TMF	Acoustically induced LPFG	80
LPFG	TMF	1529.1 to 1563.1	99%	/	/	TMF	CO_2-laser written LPFG	85
LPFG	TMFBG	1548.6	98%	72	/	Linear cavity fiber laser	CO_2-laser written LPFG	89
Mode-selective coupler	TMF	1556.3	94%	3.5	17 ns	Figure-8 fiber laser	Insertion loss 0.65 dB	97
Mode-selective coupler	TMF	1560	95%	4	1.78 ps	Seeded ring fiber laser	/	101
Mode-selective coupler	TMF	1532.5 and 1555.5	97%	0.6	0.5/0.59 ps	Ring fiber laser	Insertion loss 0.65 dB	98
Symmetric TMF coupler	TMF	1564.4	91%	1	2.552 ps	Ring fiber laser	/	99
Offset-spliced fiber	TMF	632.8	Low	/	/	TMF	/	104
Offset-spliced fiber	TMFBG	1053	94%	3.2	/	Linear-cavity fiber laser	Continuous wave	106
Offset-spliced fiber	TMFBG	1550	/	4.66	958 ns	Ring fiber laser	*Q*-switched pulse	107
Offset-spliced fiber	TMFBG	1550.5	/	/	6.87 ps	Ring fiber laser	Mode-locked pulse, insertion loss: 3 dB	105
Offset-spliced fiber	TMFBG	1056.3	96%	2.5	2.8 to 23 ns	Figure-8 fiber laser	Rectangular pulse	108
Tapered fiber	TMFBG	1548.9	/	12 to 18	5.2 to 39.2 ps	Ring fiber laser	Mode-locked pulse, insertion loss: 0.36 dB	115

Except for the aforementioned methods, several new techniques have been developed to generate CVBs in fibers or fiber lasers. Yang *et al.*[116] obtained a CVB with an arbitrary polarization rotation angle from its radial direction by manipulating either the polarization orientation or mode profile orientation of two linearly polarized Hermite–Gaussian modes in different elliptical-core few-mode fibers before their spatial superposition.

3.4 Summary of CVBs Generated in Fibers and Fiber Lasers

The generation systems and performances of CVBs using different schemes are summarized in Table 1 for a clear comparison. Each scheme has its advantages and application fields. Among them, LPFGs can be used external to the cavity or incorporated into the fiber laser, and the output CVBs exhibit the highest mode purity, typically larger than 98%. The mode-selective couplers have a broadband optical response and are frequently incorporated into fiber lasers to generate continuous-wave or pulsed CVBs, while the output power is relatively small due to the low coupling coefficient of the high-order modes. The offset-spliced fiber and tapered fiber are usually combined with TMFBGs to generate CVBs in fiber lasers. Due to the limited reflection bandwidth of TMFBGs, the duration of the pulse is usually higher than several picoseconds. By utilizing TMF with a large propagation constant difference, the first reflection spectrum of chirped TMFBGs can be broadened and is capable of supporting femtosecond pulses. Compared with the pretapered mode-selective coupler that must be precisely designed, the offset-spliced fiber, tapered fiber, and TMFBG can be easily fabricated, and the mode purity mainly depends on the reflectivity of TMFBG.

4 Generation of VBs in Fibers and Fiber Lasers

Taking the TMF as an example, it supports six modes in the vortex basis, as described in Eq. (1). Among them, the four high-order modes are VBs carrying OAM (Fig. 10):

$$\begin{aligned}
V_{21}^{+}(r,\theta) &= (\mathrm{HE}_{21}^{\mathrm{even}} + i\mathrm{HE}_{21}^{\mathrm{odd}})/\sqrt{2} = e^{i\theta}(\hat{x}+i\hat{y})F_{11}/\sqrt{2},\\
V_{21}^{-}(r,\theta) &= (\mathrm{HE}_{21}^{\mathrm{even}} - i\mathrm{HE}_{21}^{\mathrm{odd}})/\sqrt{2} = e^{-i\theta}(\hat{x}-i\hat{y})F_{11}/\sqrt{2},\\
V_{T}^{+}(r,\theta) &= (\mathrm{TM}_{01} - i\mathrm{TE}_{01})/\sqrt{2} = e^{-i\theta}(\hat{x}+i\hat{y})F_{11}/\sqrt{2},\\
V_{T}^{-}(r,\theta) &= (\mathrm{TM}_{01} + i\mathrm{TE}_{01})/\sqrt{2} = e^{i\theta}(\hat{x}-i\hat{y})F_{11}/\sqrt{2}.
\end{aligned} \tag{11}$$

As $\mathrm{HE}_{21}^{\mathrm{even}}$ and $\mathrm{HE}_{21}^{\mathrm{odd}}$ are two degenerate eigenmodes with the same propagation constant, the superposition of two modes is stable during the propagation in TMF. In contrast, TM_{01} and TE_{01} have different propagation constants, and the superposition of them (V_{T}^{+} and V_{T}^{-}) changes with the propagation distance. Thus, the circularly polarized first-order VBs are generally formed with the linear combination of $\mathrm{HE}_{21}^{\mathrm{even}}$ and $\mathrm{HE}_{21}^{\mathrm{odd}}$ modes with a $\pm\pi/2$ phase difference.[82] This is feasible for generating continuous-wave VBs that have a narrow bandwidth. For picosecond and femtosecond VBs, the HE_{11}^{x} mode couples to the TM_{01} and $\mathrm{HE}_{21}^{\mathrm{even}}$ modes, whereas the HE_{11}^{y} mode couples to the TE_{01} and $\mathrm{HE}_{21}^{\mathrm{odd}}$ modes simultaneously because the spectra usually exceed the resonant wavelength separation of the

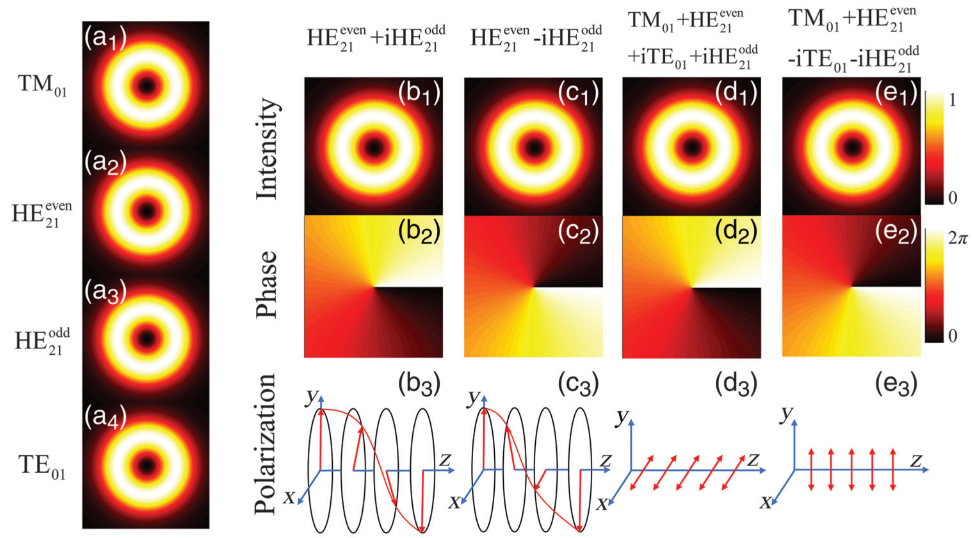

Fig. 10 Formation mechanism of VBs in TMF. (a_1)–(a_4) mode distribution of TM_{01}, HE_{21}^{even}, HE_{21}^{odd}, and TE_{01} modes. Mode distribution, phase, and polarization of (b_1)–(b_3), (c_1)–(c_3) circularly polarized VBs and (d_1)–(e_3), (e_1)–(e_3) linearly polarized VBs.

TM_{01} (TE_{01}) mode and the HE_{21}^{even} (HE_{21}^{odd}) mode. In this case, the formation of VBs is described as

$$\begin{aligned} V_x &= V_{21}^{+}(r,\theta) + V_T^{-}(r,\theta) \\ &= (\mathrm{TM}_{01} + \mathrm{HE}_{21}^{\mathrm{even}} + i\mathrm{TE}_{01} + i\mathrm{HE}_{21}^{\mathrm{odd}})/\sqrt{2} = \hat{x}e^{i\theta}F_{11}/\sqrt{2}, \\ V_y &= V_{21}^{-}(r,\theta) + V_T^{-}(r,\theta) \\ &= (\mathrm{TM}_{01} + \mathrm{HE}_{21}^{\mathrm{even}} - i\mathrm{TE}_{01} - i\mathrm{HE}_{21}^{\mathrm{odd}})/\sqrt{2} = \hat{y}e^{i\theta}F_{11}/\sqrt{2}. \end{aligned} \tag{12}$$

It is apparent that the obtained VBs are linearly polarized along the x- and y-axes, respectively.[55] The phase difference of $\pm\pi/2$ can be easily induced by a PC. According to the theoretical analysis, the formation of VBs is also based on the coupling and superposition of fiber eigenmodes. As a result, the mode couplers mentioned previously can be modified to generate VBs (Fig. 10).

4.1 Long Period Fiber Grating for Generating VBs

Dashti et al.[84] demonstrated that the OAM of the acoustic vortex can be transferred to a circularly polarized fundamental optical mode. They have created the stable ±1-order VBs directly in the TMF by coupling the fundamental mode to high-order modes using two flexural acoustic waves with orthogonal vibration directions. After that, our group analyzed the coupling behavior of the fundamental mode to four high-order modes to generate VBs based on an acoustically induced LPFG.[118] As shown in Fig. 11, the output beam delivered from a tunable laser was amplified by an EDFA and then divided into two branches by a 3-dB optical coupler. One branch was used to generate the VB while the other was a reference beam to interfere with the generated VB. For the branch of generating the VB, the beam was first coupled into a section of SMF and then passed through a tunable attenuator as well as a polarizer. After that, the linearly polarized beam was converted to a circularly polarized mode ($HE_{11}^x \pm iHE_{11}^y$) by a PC. The TMF was directly spliced to the SMF, and a mode stripper ensured the purity of circularly polarized fundamental mode. Then, the fundamental mode entered the acoustically induced LPFG and was converted to the VB ($HE_{21}^{even} \pm iHE_{21}^{odd}$) when the phase matching condition was satisfied. Simultaneously, Lu et al. reported mode-switchable generation of LP_{11} modes and ±1-order VBs based on an acoustically induced LPFG.[119] The proposed scheme can also be used to generate linearly polarized femtosecond VBs.[55]

Li et al.[120] demonstrated a controllable all-fiber VB converter in which a mechanical LPFG was employed to transform the fundamental mode to higher-order modes, and two flat slabs stressed the TMF to introduce the $\pm\pi/2$ phase difference between two higher-order modes, as shown in Fig. 12(a). Figures 12(b_1) and 12(b_3) show the field distributions of the generated VBs, which have the typical annular profiles with a dark center. Figures 12(b_2) and 12(b_4) show coaxial interference patterns of the generated VBs with the Gaussian beam. The counterclockwise and clockwise spiral interference patterns can be clearly observed from the figures, indicating that ±1-order VBs were successfully achieved from the TMF. They have also investigated the generation, conversion, and exchange of VB using helical gratings.[121] The conversion efficiency and conversion bandwidth were about 100% and 10 nm, respectively. After that, Zhao et al.[122] proposed a mode converter based on an LPFG written in the TMF to directly deliver VB and CVB.

For LPFG based on a TMF, only first-order VBs can be generated due to the limitation of the available transverse modes. Wu et al. fabricated a strong modulated LPFG written in a four-mode fiber to generate ±2-order VBs.[123] Han et al.[124] demonstrated controllable generation of circularly polarized ±1- and ±2-order VBs with two cascaded LPFGs for realizing mode conversions in four-mode fiber. After that, Zhao et al.[125] proposed an all-fiber VB generator based on a second-order helical LPFG written in a few-mode fiber, which enables direct transforming of the fundamental mode to ±2-order vortex modes with an efficiency of ~90%. More recently, ±3-order VBs were demonstrated by employing an asymmetric LPFG fabricated on six-mode fiber.[126]

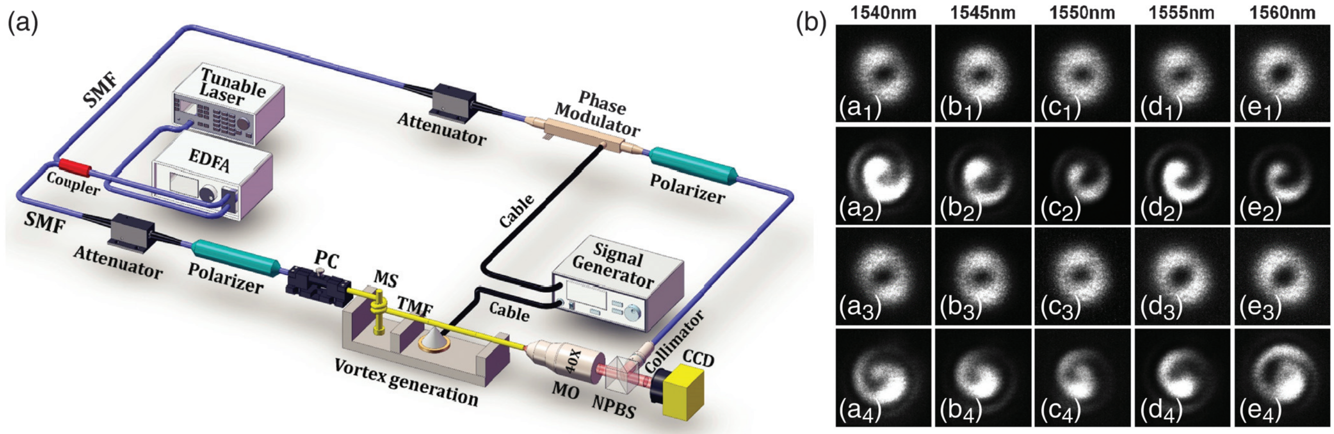

Fig. 11 Generation of VBs based on an acoustically-induced LPFG. (a) Experiment setup. EDFA, erbium-doped fiber amplifier; SMF, single-mode fiber; PC, polarization controller; MS, mode stripper; TMF, two-mode fiber; MO, micro-objective; NPBS, nonpolarizing beam splitter; CCD, charge coupled device. (b) VBs and coaxial interference patterns at wavelengths of 1540, 1545, 1550, 1555, and 1560 nm. Adapted with permission from Ref. 118 © OSA Publishing.

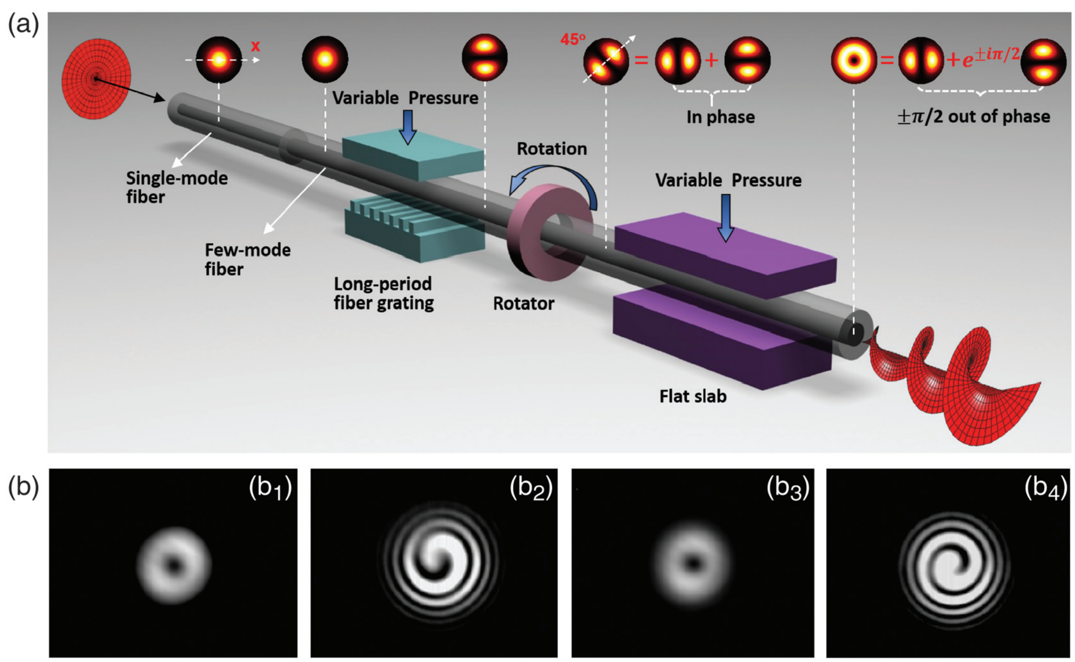

Fig. 12 (a) Principle of the VB converter based on a mechanical LPFG. Intensity profiles of (b_1) −1-order and (b_3) +1-order VB. Coaxial interference patterns of (b_2) −1-order and (b_4) +1-order VB with a Gaussian beam. Adapted with permission from Ref. 120 © OSA Publishing.

4.2 Mode-Selective Coupler for Generating VBs

The typical fused fiber coupler consists of two parallel optical fibers that have been twisted, stretched, or fused together so that the fiber cores are very close to each other and the power couples from one fiber to another fiber.[100,127] The principle of the mode-selective coupler is to phase match the fundamental mode in the SMF with high-order modes in a few-mode fiber and achieve mode conversion from the fundamental mode to the desired high-order modes. In the SMF and few-mode fiber terminals, the output beams are the fundamental and the high-order modes, respectively. The fabrication method of a mode-selective coupler for generating VB is similar to that of CVBs.[128] Wang et al.[100] demonstrated femtosecond optical VBs in an all-fiber mode-locked laser using a mode-selective coupler. The mode converter could couple the LP_{01} mode to LP_{11} (LP_{21}) mode in a broadband wavelength range. They have obtained linearly polarized ± 1 (± 2)-order VBs by combining $TM_{01} + HE_{21}^{even}$ ($HE_{31}^{odd} + HE_{31}^{even}$) and $TE_{01} + HE_{21}^{odd}$ ($HE_{01}^{even} + HE_{31}^{odd}$) with the $\pi/2$ phase difference. The durations of ± 1-order VBs and ± 2-order VBs are 273 and 140 fs, respectively. By employing a microknot resonator as the comb filter, they reported direct generation of wavelength-switchable VBs from 1546.95 to 1562.29 nm in an all-fiber erbium-doped fiber laser.[129] Recently, Yao et al.[127] found that the mode purity of the VBs was wavelength-sensitive if the input polarization of fundamental mode kept unchanged.

4.3 Fiber Taper Combined with TMFBG for Generating VBs

Continuous-wave and picosecond VBs can also be generated by exploiting SMF-TMF taper as the mode coupler and TMFBG as the mode selector.[130] In the coupling region, the light in the SMF taper couples into the TMF taper due to the strong evanescent field. Since the light field in the TMF taper deviates from the axial symmetry, parts of the HE_{11}^x and HE_{11}^y modes are converted into the $TM_{01} + HE_{21}^{even}$ and $TE_{01} + HE_{21}^{odd}$ modes while the residual mode is the fundamental mode. After that, the high-order modes are transformed into VBs by a PC, while the TMFBG works as a transverse mode selector to reflect the residual fundamental mode and export VBs. We have achieved continuous-wave and mode-locked VBs in an erbium-doped fiber laser based on three different schemes in which the mode couplers and reflectors were LPFG and fiber mirror, fiber taper, and fiber Bragg grating, and LPFG and fiber Bragg grating, respectively.[130] The operation was switchable between ± 1-order VBs by tuning the intracavity PC, as shown in Fig. 13. For the mode-locked VBs, the pulse duration was several picoseconds, which was mainly limited by the bandwidth of the TMFBG. For the continuous-wave operation, the output power exceeded 35 mW, and the VBs can directly work as optical tweezers to manipulate rhenium diselenide nanosheets.

4.4 Summary of VBs Generation in Fibers and Fiber Lasers

The aforementioned techniques are mainly focused on mode modulation in few-mode fibers or fiber lasers. Similar to the principle of the offset-splicing scheme for generating CVBs, fiber-to-fiber butt coupling was proposed to realize high-order fiber mode conversion for creating ± 1-order VBs.[131] Recently, Fu et al.[132] reported $+5$- and $+6$-order VBs by twisting a solid-core hexagonal photonic crystal fiber during hydrogen-oxygen flame heating process. Xie et al. developed an integrated fiber-based mode converter to generate VBs by attaching vortex gratings onto the facets of a few-mode fiber.[133] The grating at the input terminal of the fiber converted the Gaussian beam into the VBs, while the grating at the output terminal converted the VBs into a Gaussian beam. Such integrated (de)multiplexer has been applied for OAM fiber communication. By directly fabricating a metasurface onto the facet of a large-mode-area fiber, Zhao et al.[134] realized the excitation of both linearly polarized and circularly polarized VBs from 1480 to 1640 nm with a purity above 93%.

The mode purity and conversion efficiency are frequently adopted to evaluate the performance of generation methods. Bozinovic and Ramachandran *et al.* defined mode purity as the energy ratio of the desired mode to all modes in the fiber and proposed a measuring method by analyzing fiber output projections onto left circular and right circular polarization states.[82] The conversion efficiency is usually defined as the ratio of the output power of the desired mode to the input power of the fundamental mode (i.e., launched pump power), which is slightly different from the mode purity due to the insertion loss of the converter.[135] The generation methods and performances of VBs are summarized in Table 2. Among them, the purity of VBs based on an LPFG is higher than those of other techniques, which is similar to that of CVBs. Due to the broadband response, the mode-selective coupler can be incorporated into fiber lasers to generate ultrafast VBs. Except for a PC that is used to introduce the $\pm\pi/2$ phase difference, the coupling devices and generation systems of VBs are quite similar to that of CVBs, as summarized in a recent review article.[136]

5 Conclusion and Outlook

During the propagation in TMF, the stability of CVBs and VBs depends on the degeneracy of the four vector modes.[137] For CVBs and VBs generated in conventional TMFs or TMF lasers, the beam stability is sensitive to the experimental environment. For example, the fiber vibration and temperature fluctuation may affect the coupling behavior and thus influence the purity and power of desired beams. The operation state of CVB rests with the excited eigenmodes and is switchable between APB and RPB by changing the input polarization state. For VBs, the chirality can be controlled by tuning the phase differences between the excited high-order eigenmodes.

In polarization maintaining fibers, when the effective refractive index difference $\Delta n_{eff} > 10^{-4}$, the orthogonal polarizations of LP_{01} modes remain stable over the propagation length of 100 m.[138] Similar to the principle of the polarization maintaining fiber, the coupling coefficient between adjacent modes in TMF decreases with the increase of Δn_{eff}. For standard TMFs, the typical value Δn_{eff} is in the magnitude of 10^{-6}, and the mode purity of CVBs and VBs decreases significantly during propagation due to the coupling of constituent vector modes. Ramachandran et al.[117] demonstrated that a fiber with light field $E(r)$ and field gradients $[\partial E(r)/\partial r]$ at index steps gave a well-separated propagation constants of the TE_{01}, TM_{01}, and HE_{21} modes. Based on this guideline, they fabricated a ring-shaped fiber whose profile mirrored the mode distribution to realize long-distance propagation of CVB and VB. The Δn_{eff} of adjacent modes was higher than 1.5×10^{-4}, for example, the TM_{01} mode was separated by at least 1.8×10^{-4} from any other guided modes of the TMF. In this case, the separation of each grating resonant wavelength was larger than 80 nm, and four high-order modes can be excited independently in the vortex fiber by selecting the appropriate grating period.

The singularity beams generated in ring-shaped fiber are intrinsic solutions of the fiber transmission equation and can be transmitted in fiber for a long distance in a steady state. With the assistance of the LPFG, robust CVBs[117] and VBs[82] have been generated and propagated over 20 m in the as-prepared TMFs. For an input VB with a purity of 97%, the purity decreased only by ~10% over ~1 km propagation in the ring-shaped TMF. Based on a 1.1 km ring-shaped fiber, 400 Gb/s data transmission using four angular momentum modes at a single wavelength, and 1.6 Tb/s using two VBs modes over 10 wavelengths were achieved, indicating that VBs could provide an additional degree of freedom for data multiplexing in fiber networks.[61] In addition, this group has also proposed two methods to measure the mode purity of CVB[117] and VB[82] in TMFs and developed an air-core optical fiber that can support 12 distinct higher-order VBs over several kilometers.[139] Recently, Kim et al.[140] also demonstrated a highly germanium-doped-core optical fiber with a step-index profile that was capable of stably

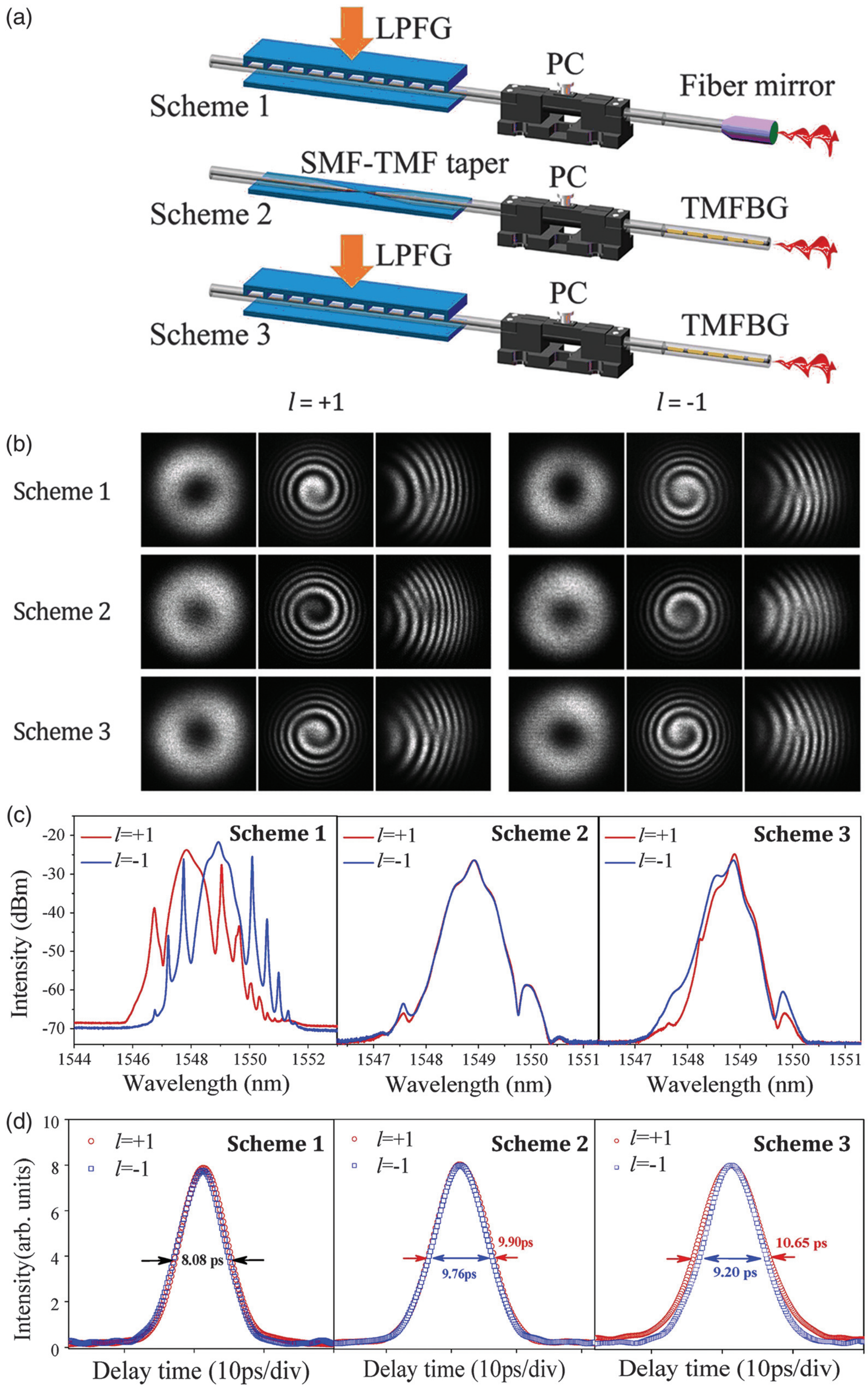

Fig. 13 (a) Mode coupling and output elements are the LPFG and fiber mirror, SMF-TMF taper and TMFBG, and LPFG and TMFBG for schemes 1, 2, and 3, respectively. (b) Intensity distributions and interference patterns, (c) optical spectra, and (d) autocorrelation traces of mode-locked vortex lasers. *l*, topological charge. Adapted with permission from Ref. 130 © AIP Publishing.

Table 2 Generation systems and performances of VBs based on different schemes.

Coupling device	Output element	Wavelength (nm)	Mode purity	Output power (mW)	Pulse duration	Generation system	Supplementary information	Ref.
LPFG	TMF	1520 to 1570	~100%	/	/	TMF	Acoustically induced LPFG	84
LPFG	TMF	1530 to 1625	97%	/	/	TMF	Mechanically induced LPFG	120
LPFG	TMF	1527	97%	/	/	Ring-shaped fiber	Mechanically induced LPFG	82
LPFG	TMF	1540 to 1560	95%	/	/	TMF	Acoustically induced LPFG	118
LPFG	LPFG	1560	95%	/	0.384 ps	TMF	Acoustically induced LPFG	55
LPFG	TMF	1548.6/1548.9	/	34.77/35.28	6.96/6.01 ps	Fiber ring laser	Mechanically induced LPFG	130
LPFG	Fiber mirror	1547.4/1547.5	/	8.9/6.99	0.90 to 5.28/0.84 to 5.28 ps	Fiber ring laser	Mechanically induced LPFG	130
Helical LPFG	Helical LPFG	1550	~100%	/	/	TMF	/	121
Helical LPFG	Helical LPFG	1550	90%	/	/	Four-mode fiber	Helical LPFG inscribed by CO_2 laser	125
Mode-selective coupler	FMF	1547.4	/	5.5	$OAM_{\pm 1}$ 273 fs; $OAM_{\pm 2}$ 140 fs	Fiber ring laser	/	100
Mode-selective coupler	TMF	1550	90%	/	/	TMF	/	127
Tapered fiber	TMFBG	1547.4/1547.5	/	32.9/35.89	6.47/6.38 ps	Fiber ring laser	/	130
Vortex grating	TMF	/	95%	/	/	TMF	Vortex grating on fiber facet	133

guiding the RPB and APB over a wide spectral range. Due to the constraints of fiber boundary conditions, the types of singular light beams in fiber are not as abundant as that in free space, and the excitation as well as extraction of desired higher-order modes in fiber remains a long-term challenge. For example, complex polarized CVBs and high-order VBs ($l > 3$) are difficult to be formed in few-mode fiber unless using specially designed fibers.[141–143]

CVBs and VBs formed in fibers and fiber lasers have found lots of special applications, such as nonlinear frequency conversion,[144–146] flattop beam generation,[147] quantum entanglement,[148] optical micromanipulation,[149,150] stimulated emission depletion (STED) microscopy,[151] optical sensing,[152] and mode-division multiplexing.[61,95,133] Furthermore, we have theoretically and experimentally presented the nanofocusing characteristic of several metal-coated fiber tips under RPB excitation in the visible band, providing an effective guideline for designing the background-free tip-enhanced Raman spectroscopy system.[153–155] Combining the azimuthal polarization characteristics of APB with the spatial symmetry characteristics of the silver nanoprism arrays,[156] the sensitivity of surface-enhanced Raman spectroscopy has been enhanced by a factor of 3.3×10^7. In addition, in the fields of fiber communications, Ryf et al. demonstrated mode-division multiplexing based on six CVBs or VBs that carried a 40 Gb/s signal over 96 km in few-mode fiber,[157] and it significantly increases the transmission capacity of fiber communication systems.

Compared with standard Gaussian beams, CVBs and VBs have unique polarization and/or phase distributions, and few-mode fibers and other specially designed fibers offer alternative media for propagating or generating such beams. We expect that special spatiotemporal optical fields can be formed by simultaneously modulating the polarization, phase, and temporal properties in few- or multiple-mode fibers and fiber lasers, and such optical fields can be further applied in fields of nonlinear fiber optics[158–164] and ultrafast strong field physics.[165–169] Compared with modulation/generation methods that have been intensively investigated, the nonlinear effects of CVB or VB are still less addressed when propagating in fibers or fiber lasers. With co-actions of mode/chromatic dispersion and nonlinearity, such CVBs or VBs may be shaped into special types of wavepackets such as spatiotemporal optical solitons.

Acknowledgments

This work was supported by the National Key R&D Program of China (2017YFA0303800), the National Natural Science Foundation of China (11874300, 11634010, 61575162, 61805277, 61675169, 91950207), the Fundamental Research Funds for the Central Universities (3102017AX009, 3102019PY002, 3102019JC008), and the Natural Science Basic Research Program of Shaanxi (2018JM6013, 2019JQ-447).

References

1. N. M. Litchinitser, "Structured light meets structured matter," *Science* **337**(6098), 1054–1055 (2012).
2. A. Forbes, "Structured light from lasers," *Laser Photonics Rev.* **13**(11), 1900140 (2019).
3. D. Cozzolino et al., "Air-core fiber distribution of hybrid vector vortex-polarization entangled states," *Adv. Photonics* **3**(4), 046005 (2019).
4. H. Sroor et al., "High-purity orbital angular momentum states from a visible metasurface laser," *Nat. Photonics* **14**(8), 498–503 (2020).
5. J. Liu et al., "Direct fiber vector eigenmode multiplexing transmission seeded by integrated optical vortex emitters," *Light-Sci. Appl.* **7**(3), 17148 (2018).

6. J. Durnin, J. J. Miceli, and J. H. Eberly, "Comparison of Bessel and Gaussian beams," *Opt. Lett.* **13**(2), 79–80 (1988).
7. T. Wulle and S. Herminghaus, "Nonlinear optics of Bessel beams," *Phys. Rev. Lett.* **70**(10), 1401–1404 (1993).
8. J. Li et al., "Simultaneous control of light polarization and phase distributions using plasmonic metasurfaces," *Adv. Funct. Mater.* **25**(5), 704–710 (2015).
9. Q. Zhan, "Cylindrical vector beams: from mathematical concepts to applications," *Adv. Opt. Photonics* **3**(1), 1–57 (2009).
10. S. Ramachandran and P. Kristensen, "Optical vortices in fiber," *Nanophotonics* **2**(5-6), 455–474 (2013).
11. Z. Chen and M. Segev, "Self-trapping of an optical vortex by use of the bulk photovoltaic effect," *Phys. Rev. Lett.* **78**(15), 2948–2951 (1997)
12. B. Y. Wei et al., "Vortex Airy beams directly generated via liquid crystal q-Airy-plates," *Appl. Phys. Lett.* **112**(12), 121101 (2018).
13. A. M. Yao and M. J. Padgett, "Orbital angular momentum: origins, behavior and applications," *Adv. Opt. Photonics* **3**(2), 161–204 (2011).
14. J. Wang, "Data information transfer using complex optical fields: a review and perspective," *Chin. Opt. Lett.* **15**(3), 030005 (2017).
15. J. Liu et al., "Multidimensional entanglement transport through single-mode fiber," *Sci. Adv.* **6**(4), eaay0837 (2020).
16. A. D. Wang et al., "Directly using 8.8-km conventional multi-mode fiber for 6-mode orbital angular momentum multiplexing transmission," *Opt. Express* **26**(8), 10038–10047 (2018).
17. M. R. Dennis, K. O'Holleran, and M. J. Padgett, "Singular optics: optical vortices and polarization singularities," in *Progress in Optics*, E. Wolf, Ed., Vol. **53**, pp. 293–363, Elsevier (2009).
18. P. Vaity and L. Rusch, "Perfect vortex beam: Fourier transformation of a Bessel beam," *Opt. Lett.* **40**(4), 597–600 (2015).
19. J. Durnin, J. Miceli, Jr., and J. H. Eberly, "Diffraction-free beams," *Phys. Rev. Lett.* **58**(15), 1499–1501 (1987).
20. G. A. Siviloglou et al., "Observation of accelerating Airy beams," *Phys. Rev. Lett.* **99**(21), 213901 (2007).
21. Z. Y. Rong et al., "Generation of arbitrary vector beams with cascaded liquid crystal spatial light modulators," *Opt. Express* **22**(2), 1636–1644 (2014).
22. N. Zhou, J. Liu, and J. Wang, "Reconfigurable and tunable twisted light laser," *Sci. Rep.* **8**(1), 11394 (2018).
23. D. Pohl, "Operation of a ruby laser in the purely transverse electric mode TE_{01}," *Appl. Phys. Lett.* **20**(7), 266–267 (1972).
24. F. Enderli and T. Feurer, "Radially polarized mode-locked Nd:YAG laser," *Opt. Lett.* **34**(13), 2030–2032 (2009).
25. L. Li et al., "High repetition rate Q-switched radially polarized laser with a graphene-based output coupler," *Appl. Phys. Lett.* **105**(22), 221103 (2014).
26. D. Naidoo et al., "Controlled generation of higher-order Poincaré sphere beams from a laser," *Nat. Photonics* **10**(5), 327–332 (2016).
27. Z. Qiao et al., "Generating high-charge optical vortices directly from laser up to 288th order," *Laser Photonics Rev.* **12**(8), 1800019 (2018).
28. B. Huang et al., "Controlled higher-order transverse mode conversion from a fiber laser by polarization manipulation," *J. Opt.* **20**(2), 024016 (2018).
29. X. L. Wang et al., "Generation of arbitrary vector beams with a spatial light modulator and a common path interferometric arrangement," *Opt. Lett.* **32**(24), 3549–3551 (2007).
30. Y. W. Zhao et al., "Intracavity cylindrical vector beam generation from all-PM Er-doped mode-locked fiber laser," *Opt. Express* **27**(6), 8808–8818 (2019).
31. K. Huang et al., "Controlled generation of ultrafast vector vortex beams from a mode-locked fiber laser," *Opt. Lett.* **43**(16), 3933–3936 (2018).
32. X. L. Wang et al., "Optical orbital angular momentum from the curl of polarization," *Phys. Rev. Lett.* **105**(25), 253602 (2010).
33. J. Lin et al., "Nanostructured holograms for broadband manipulation of vector beams," *Nano Lett.* **13**(9), 4269–4274 (2013).
34. B. Y. Wei et al., "Generating switchable and reconfigurable optical vortices via photopatterning of liquid crystals," *Adv. Mater.* **26**(10), 1590–1595 (2014).
35. A. O. Semkin and S. N. Sharangovich, "Formation of optical vortices by controllable holographic diffraction structures in liquid crystal-photopolymer compositions," *Ferroelectrics* **544**(1), 104–111 (2019).
36. P. Li et al., "Generation of perfect vectorial vortex beams," *Opt. Lett.* **41**(10), 2205–2208 (2016).
37. E. Brasselet et al., "Photopolymerized microscopic vortex beam generators: precise delivery of optical orbital angular momentum," *Appl. Phys. Lett.* **97**(21), 211108 (2010).
38. K. T. Gahagan and G. A. Swartzlander, "Optical vortex trapping of particles," *Opt. Lett.* **21**(11), 827–829 (1996).
39. X. Cai et al., "Integrated compact optical vortex beam emitters," *Science* **338**(6105), 363–366 (2012).
40. G. K. L. Wong et al., "Excitation of orbital angular momentum resonances in helically twisted photonic crystal fiber," *Science* **337**(6093), 446–449 (2012).
41. Z. Li et al., "Tripling the capacity of optical vortices by nonlinear metasurface," *Laser Photonics Rev.* **12**(11), 1870049 (2018).
42. A. Faßbender et al., "Invited article: direct phase mapping of broadband Laguerre-Gaussian metasurfaces," *APL Photonics* **3**(11), 110803 (2018).
43. S. Yu et al., "Generating multiple orbital angular momentum vortex beams using a metasurface in radio frequency domain," *Appl. Phys. Lett.* **108**(24), 241901 (2016).
44. Y. Yang et al., "Dielectric meta-reflectarray for broadband linear polarization conversion and optical vortex generation," *Nano Lett.* **14**(3), 1394–1399 (2014).
45. J. Chen, C. H. Wan, and Q. W. Zhan, "Vectorial optical fields: recent advances and future prospects," *Sci. Bull.* **63**(1), 54–74 (2018).
46. L. Zou et al., "Azimuthally polarized, passively Q-switched Yb-doped fiber laser," *Opt. Commun.* **355**, 181–185 (2015).
47. D. Lin et al., "Radially polarized and passively Q-switched fiber laser," *Opt. Lett.* **35**(21), 3574–3576 (2010).
48. R. Dorn, S. Quabis, and G. Leuchs, "Sharper focus for a radially polarized light beam," *Phys. Rev. Lett.* **91**(23), 233901 (2003).
49. S. E. Skelton et al., "Trapping volume control in optical tweezers using cylindrical vector beams," *Opt. Lett.* **38**(1), 28–30 (2013).
50. C. Min et al., "Focused plasmonic trapping of metallic particles," *Nat. Commun.* **4**(1), 2891 (2013).
51. X. Xie et al., "Harnessing the point-spread function for high-resolution far-field optical microscopy," *Phys. Rev. Lett.* **113**(26), 263901 (2014).
52. D. Liu et al., "Enhanced sensitivity of the Z-scan technique on saturable absorbers using radially polarized beams," *J. Appl. Phys.* **119**(7), 073103 (2016).
53. L. Allen et al., "Orbital angular-momentum of light and the transformation of Laguerre-Gaussian laser modes," *Phys. Rev. A* **45**(11), 8185–8189 (1992).
54. P. Lochab, P. Senthilkumaran, and K. Khare, "Near-core structure of a propagating optical vortex," *J. Opt. Soc. Am. A* **33**(12), 2485–2490 (2016).
55. W. D. Zhang et al., "Generation of femtosecond optical vortex pulse in fiber based on an acoustically induced fiber grating," *Opt. Lett.* **42**(3), 454–457 (2017).
56. Q. Zhan, "Properties of circularly polarized vortex beams," *Opt. Lett.* **31**(7), 867–869 (2006).
57. Y. Zhang et al., "Unveiling the photonic spin Hall effect of freely propagating fan-shaped cylindrical vector vortex beams," *Opt. Lett.* **40**(19), 4444–4447 (2015).
58. B. J. McMorran et al., "Electron vortex beams with high quanta of orbital angular momentum," *Science* **331**(6014), 192–195 (2011).

59. H. Ren et al., "On-chip noninterference angular momentum multiplexing of broadband light," *Science* **352**(6287), 805–809 (2016).
60. J. Wang et al., "Terabit free-space data transmission employing orbital angular momentum multiplexing," *Nat. Photonics* **6**(7), 488–496 (2012).
61. N. Bozinovic et al., "Terabit-scale orbital angular momentum mode division multiplexing in fibers," *Science* **340**(6140), 1545–1548 (2013).
62. L. S. Sui et al., "Optical multiple-image encryption based on the chaotic structured phase masks under the illumination of a vortex beam in the gyrator domain," *Opt. Express* **24**(1), 499–515 (2016).
63. Z. Shen et al., "Trapping and rotating of a metallic particle trimer with optical vortex," *APL Photonics* **109**(24), 241901 (2016).
64. J. Ng, Z. Lin, and C. T. Chan, "Theory of optical trapping by an optical vortex beam," *Phys. Rev. Lett.* **104**(10), 103601 (2010).
65. V. G. Shvedov et al., "Giant optical manipulation," *Phys. Rev. Lett.* **105**(11), 118103 (2010).
66. L. Yang et al., "Targeted single-cell therapeutics with magnetic tubular micromotor by one-step exposure of structured femtosecond optical vortices," *Adv. Funct. Mater.* **29**(45), 1905745 (2019).
67. K. Toyoda et al., "Using optical vortex to control the chirality of twisted metal nanostructures," *Nano Lett.* **12**(7), 3645–3649 (2012).
68. J. Leach et al., "Quantum correlations in optical angle–orbital angular momentum variables," *Science* **329**(5992), 662–665 (2010).
69. M. P. J. Lavery et al., "Detection of a spinning object using light's orbital angular momentum," *Science* **341**(6145), 537–540 (2013).
70. Y. W. Zhai et al., "The radial Doppler effect of optical vortex beams induced by a surface with radially moving periodic structure," *J. Opt.* **21**(5), 054002 (2019).
71. M. D. Williams et al., "Direct generation of optical vortices," *Phys. Rev. A* **89**(3), 033837 (2014).
72. S. Franke-Arnold, L. Allen, and M. Padgett, "Advances in optical angular momentum," *Laser Photonics Rev.* **2**(4), 299–313 (2008).
73. Z. Hong, J. Zhang, and B. W. Drinkwater, "Observation of orbital angular momentum transfer from bessel-shaped acoustic vortices to diphasic liquid-microparticle mixtures," *Phys. Rev. Lett.* **114**(21), 214301 (2015).
74. A. Calabuig et al., "Generation of programmable 3D optical vortex structures through devil's vortex-lens arrays," *Appl. Opt.* **52**(23), 5822–5829 (2013).
75. H. Zhang et al., "Dual-wavelength domain wall solitons in a fiber ring laser," *Opt. Express* **19**(4), 3525–3530 (2011).
76. H. Zhang et al., "Observation of polarization domain wall solitons in weakly birefringent cavity fiber lasers," *Phy. Rev. B* **80**(5), 052302 (2009).
77. X. Li et al., "Numerical investigation of soliton molecules with variable separation in passively mode-locked fiber lasers," *Opt. Commun.* **285**(6), 1356–1361 (2012).
78. L. M. Zhao et al., "Dynamics of gain-guided solitons in an all-normal-dispersion fiber laser," *Opt. Lett.* **32**(13), 1806–1808 (2007).
79. T. Wang et al., "High-order mode lasing in all-FMF laser cavities," *Photonics Res.* **7**(1), 42–49 (2019).
80. W. Zhang et al., "Cylindrical vector beam generation in fiber with mode selectivity and wavelength tunability over broadband by acoustic flexural wave," *Opt. Express* **24**(10), 10376–10384 (2016).
81. Y. Han et al., "Orbital angular momentum transition of light using a cylindrical vector beam," *Opt. Lett.* **43**(9), 2146–2149 (2018).
82. N. Bozinovic et al., "Control of orbital angular momentum of light with optical fibers," *Opt. Lett.* **37**(13), 2451–2453 (2012).
83. H. A. Haus and W. Huang, "Coupled-mode theory," *Proc. IEEE* **79**(10), 1505–1518 (1991).
84. P. Z. Dashti, F. Alhassen, and H. P. Lee, "Observation of orbital angular momentum transfer between acoustic and optical vortices in optical fiber," *Phys. Rev. Lett.* **96**(4), 043604 (2006).
85. J. Dong and K. S. Chiang, "Temperature-insensitive mode converters with CO_2-laser written long-period fiber gratings," *IEEE Photonics Technol. Lett.* **27**(9), 1006–1009 (2015).
86. M. Feng et al., "Ultra-broadband mode converter using cascading chirped long-period fiber grating," *IEEE Photonics J.* **11**(6), 7105610 (2019).
87. Y. C. Guo et al., "More than 110-nm broadband mode converter based on dual-resonance coupling mechanism in long period fiber gratings," *Opt. Laser Technol.* **118**, 8–12 (2019).
88. Y. C. Guo et al., "All-fiber mode-locked cylindrical vector beam laser using broadband long period grating," *Laser Phys. Lett.* **15**(8), 085108 (2018).
89. R. Chen et al., "High efficiency all-fiber cylindrical vector beam laser using a long-period fiber grating," *Opt. Lett.* **43**(4), 755–758 (2018).
90. Y. Zhou et al., "Resonance efficiency enhancement for cylindrical vector fiber laser with optically induced long period grating," *Appl. Phys. Lett.* **110**(16), 161104 (2017).
91. Y. Wang et al., "An all-optical, actively Q-switched fiber laser by an antimonene-based optical modulator," *Laser Photonics Rev.* **13**(4), 1800313 (2019).
92. X. Jiang et al., "Broadband nonlinear photonics in few-layer MXene $Ti_3C_2T_x$ (T = F, O, or OH)," *Laser Photonics Rev.* **12**(2), 1700229 (2018).
93. D. Li et al., "Polarization and thickness dependent absorption properties of black phosphorus: new saturable absorber for ultrafast pulse generation," *Sci. Rep.* **5**(1), 15899 (2015).
94. K. Y. Song et al., "High performance fused-type mode-selective coupler using elliptical core two-mode fiber at 1550 nm," *IEEE Photonics Technol. Lett.* **14**(4), 501–503 (2002).
95. X. H. Wang et al., "All-fiber cylindrical vector beams multiplexing through a mode-selective coupler," *IEEE J. Quantum Electron.* **55**(6), 6800408 (2019).
96. F. Wang et al., "Method of generating femtosecond cylindrical vector beams using broadband mode converter," *IEEE Photonics Technol. Lett.* **29**(9), 747–750 (2017).
97. H. Wan et al., "High efficiency mode-locked, cylindrical vector beam fiber laser based on a mode selective coupler," *Opt. Express* **25**(10), 11444–11451 (2017).
98. Z. Zhang et al., "Switchable dual-wavelength cylindrical vector beam generation from a passively mode-locked fiber laser based on carbon nanotubes," *IEEE J. Sel. Top. Quantum.* **24**(3), 1100906 (2018).
99. Y. Xu et al., "Cylindrical vector beam fiber laser with a symmetric two-mode fiber coupler," *Photonics Res.* **7**(12), 1479–1484 (2019).
100. T. Wang et al., "Generation of femtosecond optical vortex beams in all-fiber mode-locked fiber laser using mode selective coupler," *J. Lightwave Technol.* **35**(11), 2161–2166 (2017).
101. T. Wang et al., "High-order mode direct oscillation of few-mode fiber laser for high-quality cylindrical vector beams," *Opt. Express* **26**(9), 11850–11858 (2018).
102. Y. P. Huang et al., "High-order mode Yb-doped fiber lasers based on mode-selective couplers," *Opt. Express* **26**(15), 19171–19181 (2018).
103. M. Lipson, "Guiding, modulating, and emitting light on silicon—challenges and opportunities," *J. Lightwave Technol.* **23**(12), 4222–4238 (2005).
104. T. Grosjean, D. Courjon, and M. Spajer, "An all-fiber device for generating radially and other polarized light beams," *Opt. Commun.* **203**(1), 1–5 (2002).
105. D. Mao et al., "Ultrafast all-fiber based cylindrical-vector beam laser," *Appl. Phys. Lett.* **110**(2), 021107 (2017).
106. B. Sun et al., "Low-threshold single-wavelength all-fiber laser generating cylindrical vector beams using a few-mode fiber Bragg grating," *Opt. Lett.* **37**(4), 464–466 (2012).

107. J. Lin et al., "Tungsten disulphide based all fiber Q-switching cylindrical-vector beam generation," *Appl. Phys. Lett.* **107**(19), 191108 (2015).
108. B. Sun et al., "Mode-locked all-fiber laser producing radially polarized rectangular pulses," *Opt. Lett.* **40**(8), 1691–1694 (2015).
109. Y. Zhou et al., "Self-starting passively mode-locked all fiber laser based on carbon nanotubes with radially polarized emission," *Photonics Res.* **4**(6), 327–330 (2016).
110. T. Liu, S. P. Chen, and J. Hou, "Selective transverse mode operation of an all-fiber laser with a mode-selective fiber Bragg grating pair," *Opt. Lett.* **41**(24), 5692–5695 (2016).
111. S. Z. Yao et al., "All-fiber single-longitudinal-mode narrow linewidth fiber ring laser with cylindrical vector beam output," *Laser Phys. Lett.* **15**(11), 115107 (2018).
112. H. X. Li et al., "A high-efficiency all-fiber laser operated in high-order mode using ring-core Yb-doped fiber," *Ann. Phys.* **531**(10), 1900079 (2019).
113. R. Zheng et al., "An all-fiber laser generating cylindrical vector beam," *Opt. Express* **18**(10), 10834–10838 (2010).
114. Y. Zhou et al., "Actively mode-locked all fiber laser with cylindrical vector beam output," *Opt. Lett.* **41**(3), 548–550 (2016).
115. D. Mao et al., "All-fiber radially/azimuthally polarized lasers based on mode coupling of tapered fibers," *Opt. Lett.* **43**(7), 1590–1593 (2018).
116. Y. Yang et al., "All-fiber flexible generation of the generalized cylindrical vector beam (CVB) over the C-band," *IEEE J. Sel. Top. Quantum. Electron.* **26**(4), 4500307 (2020).
117. S. Ramachandran, P. Kristensen, and M. F. Yan, "Generation and propagation of radially polarized beams in optical fiber," *Opt. Lett.* **34**(16), 2525–2527 (2009).
118. W. D. Zhang et al., "Optical vortex generation with wavelength tunability based on an acoustically-induced fiber grating," *Opt. Express* **24**(17), 19278–19285 (2016).
119. J. F. Lu et al., "Dynamic mode-switchable optical vortex beams using acousto-optic mode converter," *Opt. Lett.* **43**(23), 5841–5844 (2018).
120. S. Li et al., "Controllable all-fiber orbital angular momentum mode converter," *Opt. Lett.* **40**(18), 4376–4379 (2015).
121. L. Fang and J. Wang, "Flexible generation/conversion/exchange of fiber-guided orbital angular momentum modes using helical gratings," *Opt. Lett.* **40**(17), 4010–4013 (2015).
122. Y. Zhao et al., "Mode converter based on the long-period fiber gratings written in the two-mode fiber," *Opt. Express* **24**(6), 6186–6195 (2016).
123. H. Wu et al., "All-fiber second-order optical vortex generation based on strong modulated long-period grating in a four-mode fiber," *Opt. Lett.* **42**(24), 5210–5213 (2017).
124. Y. Han et al., "Controllable all-fiber generation/conversion of circularly polarized orbital angular momentum beams using long period fiber gratings," *Nanophotonics* **7**(1), 287–293 (2018).
125. H. Zhao et al., "All-fiber second-order orbital angular momentum generator based on a single-helix helical fiber grating," *Opt. Lett.* **44**(21), 5370–5373 (2019).
126. X. D. He et al., "All-fiber third-order orbital angular momentum mode generation employing an asymmetric long-period fiber grating," *Opt. Lett.* **45**(13), 3621–3624 (2020).
127. S. Yao et al., "Tunable orbital angular momentum generation using all-fiber fused coupler," *IEEE Photonics Technol. Lett.* **30**(1), 99–102 (2018).
128. S. Pidishety et al., "Orbital angular momentum beam excitation using an all-fiber weakly fused mode selective coupler," *Opt. Lett.* **42**(21), 4347–4350 (2017).
129. J. Q. Zheng et al., "Wavelength-switchable vortex beams based on a polarization-dependent microknot resonator," *Photonics Res.* **6**(5), 396–402 (2018).
130. D. Mao et al., "Optical vortex fiber laser based on modulation of transverse modes in two mode fiber," *APL Photonics* **4**(6), 060801 (2019).
131. S. H. Li et al., "Generation of orbital angular momentum beam using fiber-to-fiber butt coupling," *IEEE Photonics J.* **10**(4), 6601607 (2018).
132. C. L. Fu et al., "High-order orbital angular momentum mode generator based on twisted photonic crystal fiber," *Opt. Lett.* **43**(8), 1786–1789 (2018).
133. Z. Xie et al., "Integrated (de)multiplexer for orbital angular momentum fiber communication," *Photonics Res.* **6**(7), 743–748 (2018).
134. Y. F. Zhao et al., "Meta-facet fiber for twisting ultra-broadband light with high phase purity," *Appl. Phys. Lett.* **113**(6), 061103 (2018).
135. D. Lin et al., "Cladding-pumped ytterbium-doped fiber laser with radially polarized output," *Opt. Lett.* **39**(18), 5359–5361 (2014).
136. H. W. Zhang et al., "Generation of orbital angular momentum modes using fiber systems," *Appl. Sci.* **9**(5), 1033 (2019).
137. S. Savovic et al., "A transmission length limit for space division multiplexing in step-index silica optical fibres," *J. Mod. Opt.* **66**(16), 1695–1700 (2019).
138. J. Noda, K. Okamoto, and Y. Sasaki, "Polarization-maintaining fibers and their applications," *J. Lightwave Technol.* **4**(8), 1071–1089 (1986).
139. P. Gregg, P. Kristensen, and S. Ramachandran, "Conservation of orbital angular momentum in air-core optical fibers," *Optica* **4**(9), 1115–1116 (2017).
140. E. M. Kim et al., "Robust vector beam guidance assisted by stress-induced cylindrical anisotropy in highly germanium-doped-core fiber," *ACS Photonics* **6**(11), 3032–3038 (2019).
141. Y. Yan et al., "Fiber structure to convert a Gaussian beam to higher-order optical orbital angular momentum modes," *Opt. Lett.* **37**(16), 3294–3296 (2012).
142. Y. Yan et al., "Efficient generation and multiplexing of optical orbital angular momentum modes in a ring fiber by using multiple coherent inputs," *Opt. Lett.* **37**(17), 3645–3647 (2012).
143. N. K. Viswanathan and V. V. G. K. Inavalli, "Generation of optical vector beams using a two-mode fiber," *Opt. Lett.* **34**(8), 1189–1191 (2009).
144. S. Ramachandran et al., "Nonlinear generation of broadband polarisation vortices," *Opt. Express* **18**(22), 23212–23217 (2010).
145. W. Zhang et al., "Tunable-wavelength picosecond vortex generation in fiber and its application in frequency-doubled vortex," *J. Opt.* **20**(1), 014004 (2018).
146. Y. S. Rumala et al., "Tunable supercontinuum light vector vortex beam generator using a q-plate," *Opt. Lett.* **38**(23), 5083–5086 (2013).
147. C. Xu et al., "All-fiber laser with flattop beam output using a few-mode fiber Bragg grating," *Opt. Lett.* **43**(6), 1247–1250 (2018).
148. N. Bozinovic et al., "Are orbital angular momentum (OAM/Vortex) states of light long-lived in fibers?" in *Front. Opt. 2011/Laser Sci. XXVII*, Optical Society of America, San Jose, California, p. LWL3 (2011).
149. G. Volpe, G. P. Singh, and D. Petrov, "Optical tweezers with cylindrical vector beams produced by optical fibers," *Proc. SPIE* **5514**, 283–292 (2004).
150. W. Qiao et al., "Approach to multiplexing fiber communication with cylindrical vector beams," *Opt. Lett.* **42**(13), 2579–2582 (2017).
151. L. Yan, P. Kristensen, and S. Ramachandran, "Vortex fibers for STED microscopy," *APL Photonics* **4**(2), 022903 (2019).
152. J. F. Yang et al., "Cylindrical vector modes based Mach-Zehnder interferometer with vortex fiber for sensing applications," *Appl. Phys. Lett.* **115**(5), 051103 (2019).
153. F. F. Lu et al., "Nanofocusing of surface plasmon polaritons on metal-coated fiber tip under internal excitation of radial vector beam," *Plasmonics* **14**(6), 1593–1599 (2019).
154. F. F. Lu et al., "Grating-assisted coupling enhancing plasmonic tip nanofocusing illuminated via radial vector beam," *Nanophotonics* **8**(12), 2303–2311 (2019).

155. M. Liu et al., "Highly efficient plasmonic nanofocusing on a metallized fiber tip with internal illumination of the radial vector mode using an acousto-optic coupling approach," *Nanophotonics* **8**(5), 921–929 (2019).
156. L. Zhang et al., "Azimuthal vector beam exciting silver triangular nanoprisms for increasing the performance of surface-enhanced Raman spectroscopy," *Photonics Res.* **7**(12), 1447–1453 (2019).
157. R. Ryf et al., "Mode-division multiplexing over 96 km of few-mode fiber using coherent 66 MIMO processing," *J. Lightwave Technol.* **30**(4), 521–531 (2012).
158. E. V. Vasilyev, S. A. Shlenov, and V. P. Kandidov, "The multifocus structure of radiation upon femtosecond filamentation of an optical vortex in a medium with an anomalous group velocity dispersion," *Opt. Spectrosc.* **126**(1), 16–24 (2019).
159. A. Dakova et al., "Vortex structures in optical fibers with spatial dependence of the refractive index," *J. Optoelectron. Adv. Mater.* **21**(7–8), 492–498 (2019).
160. H. Qin et al., "Observation of soliton molecules in a spatiotemporal mode-locked multimode fiber laser," *Opt. Lett.* **43**(9), 1982–1985 (2018).
161. L. G. Wright, D. N. Christodoulides, and F. W. Wise, "Spatiotemporal mode-locking in multimode fiber lasers," *Science* **358**(6359), 94–97 (2017).
162. D. V. Kizevetter et al., "Investigation of speckle structures formed by the optical vortices of fiber lightguides," *J. Opt. Technol* **82**(3), 174–177 (2015).
163. A. Chong et al., "Airy–Bessel wave packets as versatile linear light bullets," *Nat. Photonics* **4**(2), 103–106 (2010).
164. Y. Song et al., "Recent progress on optical rogue waves in fiber lasers: status, challenges, and perspectives," *Adv. Photonics* **2**(2), 024001 (2020).
165. X. Yang et al., "High power LP11 mode supercontinuum generation from an all-fiber MOPA," *Opt. Express* **26**(11), 13740–13745 (2018).
166. M. Kraus, J. Watzel, and J. Berakdar, "Radiation characteristics of nanoscopic structures driven by perfect optical vortex pulse," *Opt. Commun.* **427**, 390–395 (2018).
167. J. J. J. Nivas et al., "Femtosecond laser surface structuring of silicon with Gaussian and optical vortex beams," *Appl. Surf. Sci.* **418**, 565–571 (2017).
168. X. Wang et al., "Power- and polarization dependence of two photon luminescence of single CdSe nanowires with tightly focused cylindrical vector beams of ultrashort laser pulses," *Laser Photonics Rev.* **10**(5), 835–842 (2016).
169. J. Sancho-Parramon and S. Bosch, "Dark modes and Fano resonances in plasmonic clusters excited by cylindrical vector beams," *ACS Nano* **6**(9), 8415–8423 (2012).

Dong Mao is a professor at the School of Physical Science and Technology, Northwestern Polytechnical University (NPU), Xi'an, China. He received his BS degree in science from NPU in 2008 and his PhD in optical engineering from Xi'an Institute of Optics and Precision Mechanics, Chinese Academy of Sciences, Xi'an in 2014. He is the first/corresponding author of more than 40 journal papers. His research interests include ultrafast optics, nonlinear fiber optics, and nanomaterials.

Yang Zheng is currently working toward his MS degree at the School of Physical Science and Technology, NPU. His research interest is few-mode fiber lasers.

Chao Zeng is an associate professor at the School of Physical Science and Technology, NPU, Xi'an, China. He received his BS degree from Changchun University of Science and Technology in 2011 and his PhD in optical engineering from the University of Chinese Academy of Sciences in 2018. His research interests include nanophotonics, nonlinear optics, and metamaterials/metasurfaces.

Hua Lu is an associate professor at the School of Physical Science and Technology, NPU, Xi'an, China. He received his bachelor's degree from Xi'an University of Post and Telecommunications, Xi'an, China, in 2008. In January 2014, he received his PhD in optics from Chinese Academy of Sciences. In the same year, he joined the Centre for Micro-photonics, Swinburne University of Technology, Australia, as a postdoctoral fellow. His current research interests include nanophotonics, plasmonics, and guided-wave optics.

Cong Wang is currently pursuing his PhD at Shenzhen University. He received his BS degree from Shandong Normal University in 2019. His research focuses on two-dimensional nanomaterials, optical modulators, and nonlinear optics.

Han Zhang is a professor at Shenzhen University. He received his BS degree from Wuhan University in 2006 and his PhD from Nanyang Technological University in 2010. He is currently the director of Shenzhen Key Laboratory of 2D Materials and Devices and Shenzhen Engineering Laboratory of Phosphorene and Optoelectronics. His current research is on the ultrafast and nonlinear photonics of two-dimensional materials.

Wending Zhang is an associate professor at the School of Physical Science and Technology, NPU, Xi'an, China. He received his BS degree in science from NPU in 2007, his MS degree in optics, and his PhD in physics from Nankai University, Tianjin, China, in 2010 and 2013, respectively. His research interests include optical fiber-based light field modulation and plasmonic tip nanofocusing.

Ting Mei is a professor in optical engineering at NPU, Xi'an, China. He received his BS degree in optical engineering in 1988, his MS degree in optical engineering in 1991 from Zhejiang University, Hangzhou, China, and his PhD from the National University of Singapore, Singapore, in 2000. From 2000 to 2009, he was an associate professor with the Department of Electrical and Electronic Engineering, Nanyang Technological University, Singapore. From 2009 to 2013, he was a professor with the Institute of Optoelectronic Materials and Technology, South China Normal University, Guangzhou, China. From 2013 to now, he is a professor with the School of Physical Science and Technology, NPU. His current research interest includes nanophotonics, plasmonics, ultrafast nonlinear optics, and semiconductor optoelectrical material structures.

Jianlin Zhao is a professor at the School of Physical Science and Technology, NPU, Xi'an, China. He received his BS and MS degrees from NPU in 1981 and 1987, respectively. He received his PhD in optics from Xi'an Institute of Optics and Precision Mechanics, Chinese Academy of Sciences, Xi'an, in 1998. He is the director of Shaanxi Key Laboratory of Optical Information Technology, and Key Laboratory of Space Applied Physics and Chemistry, Ministry of Education. His research interests include optical information technology, micro/nano-optics, and its applications.